



The triple oxygen isotope composition of phytoliths, a new proxy of atmospheric relative humidity: controls of soil water isotope composition, temperature, CO₂ concentration and relative humidity.

Clément Outrequin¹, Anne Alexandre¹, Christine Vallet-Coulomb¹, Clément Piel², Sébastien Devidal²,
5 Amaelle Landais³, Martine Couapel¹, Jean-Charles Mazur¹, Christophe Peugeot⁴, Monique Pierre³,
Frédéric Prié³, Jacques Roy², Corinne Sonzogni¹ and Claudia Voigt¹.

¹Aix Marseille Univ, CNRS, IRD, INRA, Coll France, CEREGE, Aix-en-Provence, France

²Ecotron Européen de Montpellier, Univ Montpellier, UPS 3248 CNRS, Campus Baillarguet, Montferrier-sur-Lez, France

³Laboratoire des Sciences du Climat et de l'Environnement (LSCE/IPSL/CEA/CNRS/UVSQ), Gif-sur-Yvette, France

10 ⁴Hydrosociences Montpellier, IRD, CNRS, Univ. Montpellier, Montpellier, France

Correspondence to: Anne Alexandre (alexandre@cerege.fr)

Abstract. Continental atmospheric relative humidity is a major climate parameter whose variability is poorly understood by global climate models. Models' improvement relies on model-data comparisons for past periods. However, there are no truly quantitative indicators of relative humidity for the pre-instrumental period. Previous studies highlighted a quantitative relationship between the triple oxygen isotope composition of phytoliths, and particularly the ¹⁷O-excess of phytoliths, and atmospheric relative humidity. Here, as part of a series of calibrations, we examine the respective controls of soil water isotope composition, temperature, CO₂ concentration and relative humidity on phytolith ¹⁷O-excess. For that purpose, the grass species *Festuca arundinacea* was grown in growth chambers where these parameters were varying. The setup was designed to control the evolution of the triple oxygen isotope composition of phytoliths and all the water compartments of the soil-plant-atmosphere continuum. Different analytical techniques (cavity ring-down spectroscopy and isotope ratio mass spectrometry) were used to analyse water and silica. An inter-laboratory comparison allowed to strengthen the isotope data matching. Water and phytolith isotope compositions were compared to previous datasets obtained from growth chamber and natural tropical sites. The results show that the $\delta^{18}\text{O}$ value of the source water governs the starting point from which the triple oxygen isotope composition of leaf water, phytolith-forming water and phytoliths evolve. However, since the ¹⁷O-excess varies little in the growth chamber and natural source waters, this has no impact on the strong relative humidity-dependency of the ¹⁷O-excess of phytoliths, demonstrated for the 40-80% relative humidity range. This relative humidity-dependency is not impacted by changes in air temperature or CO₂ concentration either. A relative humidity proxy equation is proposed. Each per meg of change in phytolith ¹⁷O-excess reflects a change in atmospheric relative humidity of ca. 0.2 %. The ± 15 per meg reproducibility on the measurement of phytolith ¹⁷O-excess corresponds to a ± 3.6 % precision on the reconstructed relative humidity. The low sensitivity of phytolith ¹⁷O-excess to climate parameters other than relative humidity makes it particularly suitable for quantitative reconstructions of continental relative humidity changes in the past.

1. Introduction

The oxygen isotope composition of leaf water is an effective tool to trace processes at the soil-plant-atmosphere interface. It imprints the oxygen isotope composition of atmospheric CO₂ (Hofmann et al., 2017; Koren et al., 2019) and O₂ (Blunier et al., 2002; Brandon et al., 2020; 2018; Luz et al., 1999) used to reconstruct changes in gross primary production. The leaf water also controls the oxygen isotope composition of organic and mineral compounds formed during the plant growth (Alexandre et al., 2012; Webb and Longstaffe, 2003, 2006). This is the case for phytoliths that are micrometric hydrous amorphous silica particles polymerized in abundance in plant tissues. Preserved in soils and sediments, phytoliths can be used for paleo-vegetation and paleoclimate reconstructions.



40 The main parameters influencing the isotope composition of bulk leaf water have been determined and modeled by numerous
studies (Farquhar et al., 2007 and references therein; Cernusak et al., 2016). With regard to grasses, this composition can be
estimated assuming a mixture between a pool of unevaporated water that circulate longitudinally in the veins and a pool of
water that has been subject to evaporation in the intercellular space of the leaf stomata (Hirl et al., 2019; Leaney et al., 1985;
45 Farquhar and Lloyd, 1993; Farquhar and Gan, 2003). The volume ratio of unevaporated vs evaporated water in grass leaves,
considered in the mixing equation, can be set at 0.2 (Alexandre et al., 2019; Hirl et al., 2019) and is independent of the
transpiration rate. The ^{18}O -enrichment of the leaf water at evaporative sites, can be estimated from the Craig and Gordon
(1965) equation adapted to plant water (equation 4 from Cernusak et al. (2016) equivalent to equation 23 from Farquhar and
Lloyd (1993)). The main variables of this equation are the isotope composition of the source water absorbed by the roots,
equilibrium and kinetic fractionation factors between liquid water and water vapor, the isotope composition of atmospheric
50 water vapor, and the ratio of water vapor mole fractions in the atmosphere and at the leaf evaporation sites (w_a/w_l). This ratio
equals relative humidity (RH) when atmospheric and leaf temperatures (respectively T_{atm} and T_{leaf}) are identical. Combining
the Craig-Gordon equation with the mixing equation correctly depicts the trend of bulk leaf water ^{18}O -enrichment when RH
decreases (Alexandre et al., 2018; Gan et al., 2003; Hirl et al., 2019). However, the estimated ^{18}O -enrichment values are often
different from those observed by several ‰. This discrepancy indicates that our understanding of the parameters controlling
55 changes in the ^{18}O -enrichment of leaf water is still incomplete.

The triple oxygen isotope composition of bulk leaf water, and particularly its signature in ^{17}O -excess (as defined in section 2),
is influenced by fewer processes than $\delta^{18}\text{O}$ alone (Aron et al., 2020; Luz and Barkan, 2010; Sharp et al., 2018). Indeed, the
 ^{17}O -excess of rainwater that feeds the soil water absorbed by the roots, varies little (from -30 to 60 per meg when $\delta^{18}\text{O}$ varies
between -25 and -5 ‰; (Aron et al., 2020). This is because the ^{17}O -excess of rainwater is little sensitive to temperature (Barkan
60 and Luz, 2005; Uemura et al., 2010) or phase changes that occur during the air masses trajectories (Angert et al., 2003; Barkan
and Luz, 2007; Landais et al., 2008; Uemura et al., 2010). The ^{17}O -excess of continental atmospheric vapor, which largely
depends on that of rainwater, should also vary little from place to place, although the data are still too scarce to properly
evaluate this variability (Surma et al., 2021). Thus, changes in the ^{17}O -excess of bulk leaf water should be primarily driven by
changes in the amplitude of the kinetic fractionation due to leaf water evaporation.

65 Recent calibration studies in growth chambers (Alexandre et al., 2018, 2019) and at a tropical site (Li et al., 2017), confirmed
this assumption and highlighted a change of 2 to 4 per meg in the ^{17}O -excess of bulk leaf water for each percentage of RH.
One of the growth chamber studies showed that this translates to a change of 3 to 5 per meg in phytolith ^{17}O -excess for each
percentage of RH (Alexandre et al., 2018) and highlighted the potential of the ^{17}O -excess of fossil phytoliths to record past
changes in continental atmospheric RH. Atmospheric RH is a major climate parameter. In combination with T_{atm} , it is used to
70 estimate the concentration of the atmospheric water vapor, a major component of the water cycle and the main natural
greenhouse gas (Held and Soden, 2000; Dessler and Davis, 2010; Chung et al., 2014). However, global climate models estimate
RH from thermodynamic coupling between atmospheric water vapor and sea surface temperature (Bony et al., 2006; Stevens
et al., 2017) and its actual variability is poorly accounted for. Model-data comparisons for the pre-instrumental period are
necessary for models' improvement but face the lack of truly quantitative proxies of past RH. A promising proxy is the δD of
75 plant biomarkers (Garcin et al., 2012; Sachse et al., 2012; Rach et al., 2017; Schwab et al., 2015; Tuthorn et al., 2015) recovered
from buried soils and sediments. However, in addition to RH, the δD of plant biomarkers is dependent on other variables such
as the δD in rainwater, the plant functional type and selective degradation of the biomarkers. The ^{17}O -excess of phytoliths may
hold the potential to complement the toolbox of proxies for RH reconstructions. However, it is necessary to assess whether
and in which magnitude it can be impacted by environmental and climate parameters other than RH that changed over
80 Quaternary glacial-interglacial cycles (Govin et al., 2014; IPCC Staff., 2007). This applies to T_{atm} that drives the difference
between T_{atm} and T_{leaf} , and hence the equilibrium fractionation between liquid water and water vapor, and the atmospheric
concentration of CO_2 (CO_2) that drives the stomatal conductance and hence the kinetic fractionation in leaf water during



transpiration. The impact of changes in the triple oxygen isotope composition of soil water and atmospheric water vapor on the triple oxygen isotope compositions of leaf water and phytoliths needs also to be examined.

85 To address these issues, we present the results of a new growth chamber experiment in which the grass species *Festuca arundinacea* (*F. arundinacea*) was grown under variable conditions of RH, T_{atm} and CO_2 mimicking past and present climate conditions in tropical areas. The setup was designed to monitor the evolution of the triple oxygen isotope composition of all the water compartments in the soil-plant-atmosphere continuum. Phytolith isotope compositions were analyzed. The isotope data are compared to a previous growth chamber experiment and two datasets obtained from phytolith samples collected along
 90 a RH transect in West Africa (Alexandre et al., 2018) and a new isotope monitoring at the soil-plant interface carried out at the AMMA-CATCH natural observatory in Benin (West Africa) (this study).

2. Fractionation and notation in the triple oxygen isotope system

In the triple oxygen isotope system, the mass-dependent fractionation factors between two phases A and B ($^{17}\alpha_{A-B}$ and $^{18}\alpha_{A-B}$) are related by the exponent θ_{A-B} , which is expressed as:

95
$$^{17}\alpha_{A-B} = (^{18}\alpha_{A-B})^\theta \quad (1)$$

or

$$\theta_{A-B} = \ln^{17}\alpha_{A-B} / \ln^{18}\alpha_{A-B} . \quad (2)$$

The value of θ equals 0.529 for liquid water-water vapor equilibrium (θ_{equil} ; Barkan and Luz, 2005) and 0.518 for water vapor diffusion in air (θ_{diff} ; Barkan and Luz, 2007). While θ applies to a particular well constrained physical process, the term λ is used when several fractionation processes occur at the same time. In the $\delta^{18}O$ vs $\delta^{17}O$ space, λ represents the slope of the line linking $\Delta^{17}O_{A-B}$ to $\Delta^{18}O_{A-B}$ with

100

$$\lambda_{A-B} = \Delta^{17}O_{A-B} / \Delta^{18}O_{A-B}, \quad (3)$$

$$\Delta^{17}O_{A-B} = \delta^{17}O_A - \delta^{17}O_B \quad (4)$$

and

105
$$\delta^{17}O = \ln(\delta^{18}O + 1) \quad (5)$$

where $\delta^{*}O = (^{*}O/^{16}O)_{sample} / (^{*}O/^{16}O)_{standard} - 1$. * stands for 18 or 17.

When water evaporates, three processes interplay in the leaf boundary layer, as conceptualized by the Craig and Gordon model (Craig and Gordon, 1965). These processes can be depicted in the $\delta^{17}O$ vs $\delta^{18}O$ space as follows: (1) water-vapor equilibrium fractionation, which is temperature-dependent (Majoube, 1971), drives the isotope composition of leaf water along a line of a slope θ_{equil} ; (2) vapor diffusion in air, which is dependent on RH (or more specifically on w_a/w_i), drives the isotope composition of leaf water along a line of a slope θ_{diff} ; (3) exchange between leaf water and atmospheric water vapor, which decreases from turbulent to laminar and molecular vapor transport, and from high to low atmospheric water vapor concentration, drives the isotope composition of leaf water along a mixing curve linking the evaporated water and the atmospheric water vapor compositions. The combination of these processes leads to the ^{17}O -excess of evaporated leaf water, describing the departure of $\delta^{17}O$ from a reference line with a slope λ of 0.528, equivalent to the slope of the Global Meteoric Water Line (GMWL, expressed as $\delta^{17}O = 0.528 \times \delta^{18}O + 0.033$, Luz and Barkan, 2010). Thus, ^{17}O -excess is expressed as:

110

$$^{17}O\text{-excess} = \delta^{17}O - 0.528 \times \delta^{18}O. \quad (6)$$

The difference of ^{17}O -excess between A and B is expressed hereafter by $^{17}O\text{-excess}_{A-B}$. Since the value of 0.528 is close to the θ_{equil} value (0.529), measuring the ^{17}O -excess of water is very suitable for quantifying kinetic fractionation due to evaporation.



120 For the silica–water couple at equilibrium, the evolution of the exponent λ ($\lambda_{\text{Silica-water}}$) with temperature has been synthesized
from data and can be calculated from equation 10 in [Sharp et al. \(2016\)](#). For the 5–35°C temperature range, $\lambda_{\text{Silica-water}}$ equals
0.524 ± 0.0002, in agreement with the theoretical $\theta_{\text{Silica-water}}$ values (Cao and Liu, 2011).

3. Materials and Methods

3.1. Growth chamber experimental setup

125 *F. arundinacea*, commonly referred to as tall fescue, is a globally distributed invasive grass species, widely used as forage
(Gibson and Newman, 2001), and can adapt to a wide range of climatic conditions. Three growth chambers with a regulation
of light intensity, T_{air} , RH and CO_2 were used to cultivate the tall fescue in three soil containers at the Microcosms platform of
the Montpellier European Ecotron (France). The growth chambers as well as the growth protocol, described in detail in
Appendix A, were adapted to allow for the monitoring of the isotope composition of all the water compartments in the soil-
130 plant-atmosphere continuum (Fig. 1). The difference between the isotope composition of the water used for soil irrigation
(6.55 ‰ and 29 per meg for $\delta^{18}\text{O}$ and ^{17}O -excess, respectively) and that of the water fogged into the chamber atmosphere (-
5.64 ‰ and 17 per meg for $\delta^{18}\text{O}$ and ^{17}O -excess, respectively) were set close to the water liquid-vapor equilibrium
fractionation value characteristic of natural systems (e.g. $\Delta^{18}\text{O}$ ranging from 9.65 to 9.06 ‰ between 20 and 28°C; Majoube,
1971).

135 Three treatments which consisted in seven combinations of RH (40, 60 and 80%), T_{air} (20, 24 and 28 °C) and CO_2 (200, 300
and 400 ppm) were applied to 18 fescue regrowths (two to three replicates per climate combination), as described in Table 1.
At the end of each regrowth (lasting between 11 and 26 days), the fescue canopy was harvested. On 32 ± 24 g of fresh weight
of fescue leaves (average per regrowth), four grams were immediately inserted into glass gastight vials for leaf water extraction,
while the remaining biomass was dried at 50°C and kept for phytolith extraction. The humid air of each of the three growth
140 chambers was continuously pumped via three heated lines and sent to a laser spectrometer for sequential analyses. The
irrigation, soil and fogged waters were sampled before each regrowth for analyses. The volume of irrigation water consumed
by transpiration was estimated (Sup. mat. 1).

3.2. Water vapor and liquid water triple oxygen isotope analyses

The humid air of the chambers was analyzed at Ecotron by Wavelength-Scanned Cavity Ring Down Spectroscopy (CRDS)
145 with a Picarro L2140-i spectrometer operated in ^{17}O -excess mode. For each chamber, the water vapor in the air was measured
every second over a 420 min period before switching to the next chamber using a 16-port distribution manifold (Picarro
A0311). The raw data were averaged over 80 minutes, which resulted in 5 averages per vapor measurement period. Before
each vapor measurement period three working standards of liquid water were analyzed for calibration. The liquid
measurements consisted of ten injections per vial with the first six being discarded to account for memory effects. For each
150 treatment, the concentration of the working standards of water vaporized into the analyzer was set to be equal to the
atmospheric water vapor concentration in the chamber. The linear regression obtained using the three water standards was
used to calibrate the vapor measurements. The precision for the liquid water measurements was 0.02 ‰ and 12 per meg for
 $\delta^{18}\text{O}$ and ^{17}O -excess, respectively (1 s.d., $n = 21$). In order to estimate the background noise for each climate combination,
the atmospheric water vapor fogged from a constant water source into the empty chamber (without fractionation) was measured
155 (except for the growth at 300 ppm CO_2). The precision on the vapor measurements of 80 min was 0.004 ‰ for $\delta^{18}\text{O}$, and lower
than 10 per meg for ^{17}O -excess (1 s.d., $n=19$).

The irrigation, soil and fogged water samples were analyzed at CEREGE (France) also using a Picarro L2140-i laser
spectrometer (same configuration as at Ecotron). Each measurement run included three groups of three working standards for



160 calibration, three replicates of an additional working standard for quality assurance (QA), and three replicates per water sample, with eight injections per vial. The two first injections were not considered. Each measurement was corrected for a memory effect (Vallet-Coulomb et al., in revision for *Rapid Communications in Mass Spectrometry*). The precision on the QA value measurement was 0.02‰ for $\delta^{17}\text{O}$ and $\delta^{18}\text{O}$ and 11 per meg for ^{17}O -excess (1 s.d.; $n = 7$ measurement sessions). The averaged difference from the reference composition of the QA was 0.02‰, 0.03‰ and 1 per meg, for $\delta^{17}\text{O}$, $\delta^{18}\text{O}$ and ^{17}O -excess, respectively.

165 Bulk water was extracted from the fescue leaves using a fluorination line and analyzed with a dual inlet IRMS (ThermoQuest Finnigan MAT 253 mass spectrometer) at LSCE (France), following the procedure previously detailed in Landais et al. (2006). The measurement precisions (2 runs of 24 dual inlet measurements) were 0.1‰ for d^{18}O and d^{17}O and 6 per meg for ^{17}O -excess.

170 All water isotope compositions were normalized on the VSMOW-SLAP scale, with an assigned SLAP ^{17}O -excess value of zero, following the recommendations of Schoenemann et al. (2013). A comparison between CEREGE, Ecotron and LSCE water measurements of the same laboratory standards was performed. Results are presented in Table B1. Differences between the laboratories were lower than 0.2 ‰, 0.1 ‰ and 10 per meg for $\delta^{18}\text{O}$, $\delta^{17}\text{O}$ and ^{17}O -excess, respectively.

3.3 Phytolith extraction, counting and triple oxygen isotope analyses

175 Phytoliths were extracted from plants following a protocol detailed in Corbinau et al. (2013). Chemical removal of carbonate and organic compounds at 70 °C resulted in high-purity phytolith concentrates. Phytolith samples of 1.6 mg were then dehydrated under a flow of N_2 at 1100 °C (Chapligin et al., 2010) to prevent the formation of siloxane from silanol groups during dehydroxylation. Molecular O_2 was extracted using the IR Laser-Heating Fluorination Technique at CEREGE (Alexandre et al., 2006; Crespin et al., 2008; Suavet et al., 2010). At the end of the procedure, the gas was passed through a -114°C slush to refreeze any molecule interfering with the mass 33 (e.g., NF potentially remaining in the line). Analyses of quartz and phytolith working standards with and without the slush showed that this step is essential to get reproducible ^{17}O -excess data. The gas was directly sent to the dual-inlet mass spectrometer (ThermoQuest Finnigan Delta V Plus). Each gas sample was run twice. Each run consisted of eight dual inlet cycles (integration time of 26 seconds). A third run was performed when the standard deviation (s.d.) on the first two averages was higher than 15 per meg for ^{17}O -excess.

185 The composition of the reference gas was determined against NBS28. The sample measurements were corrected on a daily basis using a quartz laboratory standard analyzed at the beginning of the day until a ^{17}O -excess plateau was reached, and again in the middle and at the end of the day. As recommended by Sharp and Wostbrock (2021) isotope compositions obtained from the analyses of NBS28 and six working standards (including phytolith standards) at CEREGE were compared to those obtained from the same standards measured at the University of New Mexico (UNM), where the data are directly calibrated relative to VSMOW-SLAP. The inter-laboratory comparison is presented in Table C1. The averaged CEREGE-UNM ^{17}O -excess offset is -25 per meg and does not evolve with $\delta^{18}\text{O}$. This offset is comparable to the ± 24 per meg average offset to VSMOW-SLAP standardized data obtained by other laboratories (Herwartz, 2021). Since this offset is larger than the data precision (15 per meg), the silica data obtained at CEREGE were corrected by adding 20 per meg to the measured d^{17}O value (which is equivalent to adding 20 per meg to the d^{17}O or ^{17}O -excess values). The data previously presented in Alexandre et al. (2018 and 2019) were corrected accordingly. This correction allowed robust comparisons between silica and water isotope compositions.

195 The reproducibility from $\delta^{18}\text{O}$ and ^{17}O -excess measurements of the quartz laboratory standard was 0.13 ‰ and 12 per meg, respectively (1 s.d., $n = 21$ aliquots). For the phytolith samples, the averaged reproducibility from $\delta^{18}\text{O}$ and ^{17}O -excess measurements was 0.34 ‰ and 9 per meg, respectively (1 s.d., 2 to 3 aliquots). The reproducibility from phytolith ^{17}O -excess measurements was always lower than 15 per meg.



It was recently suggested that the dehydration step required before analyzing biogenic hydrous silica may induce an isotope fractionation biasing the ^{17}O -excess values (Herwartz, 2021). Arguments for the absence of significant isotope fractionation during the high-temperature dehydration under N_2 flow step are presented in Appendix C.

Phytoliths obtained from three regrowths with different RH were mounted on microscope slides in Canada Balsam for counting at a 600 X magnification. The percentage of epidermal Long cell relative to Short and Long cell phytolith types was calculated (Alexandre et al., 2018). Two counts of the same assemblage gave a difference of 1 %.

205 **3.4. Independent growth chamber and natural datasets used for comparison**

To examine the effect of the soil water isotope composition on that of phytoliths, the results from the growth chamber experiment were compared with two datasets published in Alexandre et al. (2018): 1) the first dataset includes isotope compositions of leaf water and phytoliths of *F. arundinacea* grown at Ecotron in growth chambers where RH was varied in a similar way to the current RH treatments and T_{atm} was set constant at 25°C. In the setup of this growth chamber experiment, 210 the isotope composition atmospheric water vapor was not measured. The isotope composition of the irrigation water (-5.58 ‰ and 26 per meg for $\delta^{18}\text{O}$ and ^{17}O -excess, respectively) was depleted relative to the recent growth chamber experiment but closer to natural waters. The fogged water had the same isotope composition as the irrigation water, similar to the one used in this study; 2) the second dataset includes isotope compositions of phytoliths extracted from soil tops collected along a vegetation and RH transect in West Africa. The vegetation is represented by savannas and humid forests and soil phytoliths 215 are from grasses and trees. Rainfall $\delta^{18}\text{O}$ weighted monthly means at the sampling locations ranged from -1.5 to -4.5 ‰ (Online Isotopes in Precipitation Calculator-version OIPC2- 2; Bowen et al., 2005). Monthly mean RH extracted from the Climate Research Unit (CRU) 1961–1990 time series ranged from 57 to 82% (Alexandre et al., 2018).

Additionally, a new dataset was obtained from an ongoing monitoring at the AMMA-CATCH natural observatory (Galle et al., 2018) in Benin (West Africa) where dry forest and savannas prevail under a tropical humid climate. The mean annual rainfall 220 is 1300 mm with 60% occurring during the rainy season between July and September. The mean annual T_{atm} is 26°C. RH ranges from 10 to 20% during the dry season and from 50 to 80% during the rainy season. The observatory is equipped with a meteorological station, providing hourly records of T_{atm} and RH. The rainwater was collected continuously during the grass growing period and its isotope composition was analyzed (section 3.2). Two grass species (*Hypparrhenia involucreta* and *Andropogon gayanus*) were collected at the beginning and in the middle of the rainy season in the dry forest and the savanna 225 plots. Phytoliths were extracted from the stems that are supposed to be non-transpiring organs, and analyzed (section 3.3).

4. Results

4.1 Effectiveness of the growth chamber monitoring

For each growth, the water fluxes and the isotope compositions of the water compartments in the soil-plant-atmosphere continuum are presented in supplementary material 1 and illustrated on Fig. 1. The volumes of transpired water estimated by 230 isotope mass-balance are very close to the measured volumes (the slope of the correlation (not shown) is 1.0.; $r^2 = 0.97$), supporting the effectiveness of the monitoring. During the growth, the vapor $\delta^{18}\text{O}$ increases linearly (Fig. 1), in response to the increasing contribution of transpired water to the atmosphere, unfractionated relative to the irrigation water (Welp et al., 2008). Since the ^{17}O -excess of the irrigation water is close to that of fogged water the transpiration has little effect on the ^{17}O -excess of the atmospheric vapor.

235 **4.2 Biomass productivity, transpiration and phytolith content**

Considering all the regrowths, the biomass productivity and phytolith content range from 1.1 ± 0.2 to 3.5 ± 0.9 g/day and from 1.4 ± 0.4 to 4.4 ± 1.7 % dry weight, respectively (Table 1). The transpiration rate measured at the end of each regrowth ranges



from 0.2 to 0.6 L/day (Sup. mat. 1.1). For each of these variables, there is a high variability between replicates which may explain the low correlation with the vapor pressure deficit (VPD). Noteworthy, the averaged phytolith content is negatively correlated with the biomass productivity ($r^2=0.7$) and the transpiration rate ($r^2=0.4$). In the phytolith assemblages, the percentage of the Long cell phytolith type ranges from 16 to 31%, increasing with VPD ($r^2=0.9$).

4.3 Leaf water isotope composition response to RH, T_{air} and CO_2 changes

Evolutions of the triple oxygen isotope composition of leaf water with variable RH, T_{air} , CO_2 and the associated VPD (Table 2) are illustrated on Fig. 2. The 80 to 40% decrease of RH, corresponding to a 1.2 kPa increase of VPD, leads to a 5.9 ‰ increase in $\delta^{18}\text{O}$ and a 108 per meg decrease in ^{17}O -excess, which is characteristic of an evaporation trend. There is no impact of CO_2 changes on the $\delta^{18}\text{O}$ and ^{17}O -excess of leaf water. The increase in T_{atm} from 20 to 28°C, which corresponds to a 0.6 kPa increase of VPD, comes with a 5.1 ‰ decrease of $\delta^{18}\text{O}$, which is opposite to an evaporative kinetic fractionation trend. The ^{17}O -excess does not change significantly with variable T_{atm} . The fractionation between irrigation and leaf waters values is presented in Table 2. There is no significant trend in the triple oxygen isotope fractionation coefficient λ between leaf water and irrigation water ($\lambda_{\text{LW-IW}}$) with RH.

4.4 Phytolith isotope composition response to RH, T_{air} and CO_2 changes

Changes in the triple oxygen isotope compositions of phytoliths with RH, T_{air} , CO_2 and the associated VPD values (Table 2) are illustrated on Fig. 2. Given the $\delta^{18}\text{O}$ and ^{17}O -excess precision ranges, no changes are observed when T_{atm} or CO_2 vary. The evaporation trend noted for leaf water is also observed for phytoliths but at a higher rate: the $\delta^{18}\text{O}$ of phytolith increases from 36.0 ± 0.2 to 48.6 ± 1.4 ‰ with RH decreasing from 80 to 40 %. In the same time, the ^{17}O -excess of phytoliths decreases from -177 ± 2 to -336 ± 22 per meg.

The apparent fractionation between leaf water and phytoliths ($\Delta^{18}\text{O}_{\text{Phyto-LW}}$) is presented in Table 2. Between 80 and 60% RH, it is invariable ($\Delta^{18}\text{O}_{\text{Phyto-LW}}$ equals to 25.27 ± 1.88 ‰ and 26.77 ± 0.35 ‰ at 80 and 60% RH, respectively) but lower than expected for equilibrium fractionation between water and silica ($\Delta^{18}\text{O}_{\text{Silica-water}} = 31$ and 33 ‰ for 26 and 18°C, according to Dodd and Sharp (2010)). At 40% RH, $\Delta^{18}\text{O}_{\text{Phyto-LW}}$ is similar to the equilibrium value. The value of $\Delta^{18}\text{O}_{\text{Phyto-LW}}$ does not change significantly from 28 to 24°C but decreases by 3.2 ‰ from 24°C to 20°C. This decrease is opposed to the increasing fractionation expected for equilibrium when temperature decreases. It is also opposed to the increase in the fractionation between irrigation and leaf waters ($\Delta^{18}\text{O}_{\text{LW-IW}}$). This translates into invariable fractionation between irrigation water and phytoliths ($\Delta^{18}\text{O}_{\text{Phyto-IW}}$). Overall, the λ value calculated for the leaf water-phytolith couple ($\lambda_{\text{Phyto-LW}}$) averages 0.522 ± 0.0005 (Table 2).

The isotope compositions of the stem phytoliths extracted from the two grass species collected at the AMMA-CATCH observatory are presented in Table 3. The isotope composition of the stem phytolith-forming waters is assumed to be close to the amount-weighted isotope composition of rainfall averaged for the growing season preceding the grass sampling. The obtained fractionation values for the rainwater-phytolith couple, i.e. $\Delta^{18}\text{O}_{\text{Phyto-RW}}$ and $\lambda_{\text{Phyto-RW}}$, are 31.18 ± 0.63 (1 s.d.) ‰ and 0.523 ± 0.0004 , respectively. They are almost identical to the equilibrium values of 30.78 ± 0.39 ‰ and 0.524 ± 0.0002 calculated for $\Delta^{18}\text{O}_{\text{Silica-water}}$ and $\lambda_{\text{Silica water}}$ after Dodd and Sharp (2010) and Sharp et al. (2016), respectively.

5. Discussion

5.1 Parameters controlling the triple oxygen isotope composition of leaf water

In order to consider the parameters responsible for the changes in the isotope composition of bulk leaf water, the $\delta^{18}\text{O}$ and ^{17}O -excess values were predicted for the current and 2018 growth chamber experiments using the modeling method described



in section 1. T_{leaf} was assumed to be 2°C lower than T_{atm} (Alexandre et al., 2019b). For the 2018 experiment, since the vapor was not measured, the associated $\delta^{18}\text{O}$ and ^{17}O -excess values were set similar to those of the irrigation water as both fogged and irrigation waters came from the same tap water. The calculations are detailed in Sup. mat. 1.2.

Fig. 3 shows the observed and predicted $\delta^{18}\text{O}$ and ^{17}O -excess values of leaf water, for the CO_2 , T_{air} and RH treatments. For the CO_2 treatment, the small amplitude of changes in stomatal conductance, estimated from the CO_2 concentration (Barillot et al., 2010 and Ainsworth and Rogers, 2007), has no effect on the predicted $\delta^{18}\text{O}$ and ^{17}O -excess of leaf water, in agreement with the observations. For the T_{air} treatment, the model does not predict any significant change in $\delta^{18}\text{O}$ and ^{17}O -excess, in disagreement with the high $\delta^{18}\text{O}$ value observed at 20°C. $T_{\text{air-leaf}}$ is difficult to measure or estimate, in growth chambers as well as outdoor, which certainly accounts for the inaccuracy frequently encountered when the $\delta^{18}\text{O}$ of leaf water is modelled.

However, in the present case, different-than-expected $T_{\text{air-leaf}}$ values would move the $\delta^{18}\text{O}$ and ^{17}O -excess of leaf water along the predicted line and cannot account for the offset in $\delta^{18}\text{O}$ only observed at 20°C. For the current and 2018 RH treatments, the trends described by the $\delta^{18}\text{O}$ and ^{17}O -excess of leaf water when RH changes are correctly predicted although some $\delta^{18}\text{O}$ and ^{17}O -excess values are significantly lower than expected from the model. For example, for the current RH treatment, the $\delta^{18}\text{O}$ at 40% is 6‰ lower than predicted. For the 2018 RH treatment, the ^{17}O -excess can be 50 per meg lower than predicted.

These model-data discrepancies could be related, as previously suggested (Alexandre et al., 2018; Li et al., 2017), to the misestimation of the isotope composition of the atmospheric water vapor. The isotope composition of the vapor was measured close to the leaves in the current growth chamber setup. However, it may be heterogeneous at the millimetric scale around the leaves. In addition, the high variability of the isotope composition of leaf water observed between replicates suggests that despite the precautions taken to harvest the grass regrowths as quickly as possible, changes in climatic parameters and isotope composition of the atmospheric water vapor when moving the containers outside the chambers may have a little biased the isotope compositions of the leaf waters. Outside atmospheric vapor with $\delta^{18}\text{O}$ and ^{17}O -excess values lower than inside the chamber would lower the $\delta^{18}\text{O}$ and ^{17}O -excess of the leaf water during the mixing step of the evaporation process (section 2).

Fig. 4 shows the leaf water isotope compositions at 40, 60 and 80% RH for the current and 2018 growth chamber experiments as well as the isotope compositions of the source water (i.e. irrigation water) in the ^{17}O -excess vs $\delta^{18}\text{O}$ space. In agreement with the observations, sensitivity tests using the bulk leaf water model show that the isotope compositions of the source water (or the irrigation water) and the difference in composition between the source water and the atmospheric water vapor control the starting point from which the isotope composition of the leaf water evolves. When RH decreases, the isotope composition of the source water becomes the overriding factor. Because the ^{17}O -excess values of the source waters in the current and 2018 experiments are similar, this has little effect on the dependency on RH of the ^{17}O -excess of leaf water.

This dependency is expressed for the current experiment by (eq. 7)

$$^{17}\text{O-excess}_{\text{LW-SW}} \text{ (per meg)} = 2.8 (\pm 0.2) * \text{RH} (\%) - 285 (\pm 14) \quad (r^2=0.97; \text{p-value} < 0.0001), \quad (7)$$

where $^{17}\text{O-excess}_{\text{LW-SW}}$ is the difference of ^{17}O -excess between the leaf water (LW) and the source water (SW). Given the precision ranges, this equation is close to (eq. 8)

$$^{17}\text{O-excess}_{\text{LW-SW}} \text{ (per meg)} = 2.1 (\pm 0.7) * \text{RH} (\%) - 248 (\pm 44) \quad (r^2=0.55; \text{p-value} < 0.05) \quad (8)$$

recalculated from the 2018 growth chamber dataset.

5.2 Parameters controlling the triple oxygen isotope composition of phytoliths

As observed in Fig. 2 and reported in the section 4, T_{air} and CO_2 changes do not affect the ^{17}O -excess of phytoliths. With regard to T_{air} , this is the consequence of θ_{equil} and $\lambda_{\text{silica-water}}$ changing little with temperature. For instance, using an equilibrium $\Delta^{18}\text{O}_{\text{silica-water}}$ value estimated from Dodd and Sharp (2010) and an equilibrium $\lambda_{\text{silica-water}}$ value of 0.524 (Sharp et al., 2016), the ^{17}O -excess of silica formed from a given water should vary by less than 10 per meg from 18 to 26 °C, which is lower than the analytical precision range.



The phytolith triple oxygen isotope compositions at 40, 60 and 80% RH are shown in Fig. 4 for the current and 2018 growth chamber experiments. The regression lines established from the isotope compositions are characteristic of evaporation trends. They are almost parallel for both experiments (Student's t-test). As for the leaf water, contrasting source water $\delta^{18}\text{O}$ values and differences between source water and water vapor $\delta^{18}\text{O}$ values can explain their offset in $\delta^{18}\text{O}$. The isotope compositions of soil phytoliths from the 2018 natural transect sampling and stem phytoliths from the AMMA-CATCH site are also shown on Fig. 4. The isotope compositions of the soil phytoliths are distributed on and around the 2018 growth chamber line. The isotope compositions of the stem phytoliths are also located closer to the 2018 growth chamber line than to the current one. This can be explained by the proximity of the $\delta^{18}\text{O}$ values of rainwater at the natural sites (from -1.5 to -4.5 ‰ for the natural transect (Alexandre et al., 2018) and from -1.9 to -4.3 ‰ for the AMMA-CATCH site) to the $\delta^{18}\text{O}$ of the irrigation water of the 2018 experiment (-5.6 ‰). These data support that as for bulk leaf water, the isotope composition of the source water and the difference in composition between source water and the water vapor govern the starting point from which the triple oxygen isotope compositions of grass phytoliths evolve with decreasing RH. Since the range of ^{17}O -excess variation in the source waters and the atmospheric water vapor is narrow in the growth chambers and is expected to be narrow at the natural sites, the source water has little impact on the RH-dependency of the ^{17}O -excess of phytoliths.

Fig. 4 shows that the phytolith regression lines obtained from the 2018 and current growth chamber experiments are shifted in ^{17}O -excess while this is not the case for the leaf water lines. This can be linked to the mean value of $\lambda_{\text{Phyto-LW}}$ calculated for the current growth chamber experiment (0.522 ± 0.0005), that is slightly lower than the mean value recalculated for the 2018 experiment (0.523 ± 0.0012 ; Sup. mat. 1.3). Previous measurement and modelling of the evolution of the triple oxygen isotope composition of the grass leaf water and phytoliths with leaf length suggested that $\lambda_{\text{Phyto-LW}}$ decreased from the base (0.523) to the apex (0.521) of the leaves. The mean value of the bulk grass leaf was 0.522 (recalculated from Alexandre et al., 2019). The increasing distance from the $\lambda_{\text{Silica-water}}$ equilibrium value of 0.524 was interpreted as the sign of an apparent kinetic fractionation increasing from the base to the apex (Alexandre et al., 2019). The proximity of $\Delta^{18}\text{O}_{\text{Phyto-RW}}$ and $\lambda_{\text{Phyto-RW}}$ averaged values obtained for phytoliths from the grass stem samples collected at the AMMA-CATCH site (section 4.4) to the $\Delta^{18}\text{O}_{\text{Silica-water}}$ and $\lambda_{\text{Silica-water}}$ equilibrium values rules out a fractionation occurring systematically during high-temperature dehydration. It rather suggests that the processes behind the apparent kinetic fractionation are limited when evaporation is restricted, as it is the case in stems.

Heterogeneous silicification processes may contribute to an apparent kinetic fractionation between evaporated leaf water and silica. At least two patterns of silicification in grass leaf epidermis have been reported (Kumar et al., 2017). Short cells are among the first types of cells to be silicified, sometimes even before the leaf transpires. The process appears metabolically controlled and does not depend on the transpiration rate. To the contrary, long cells silicify only when the plant starts to transpire and all the more so as the transpiration rate increases. If the isotope composition of leaf water changing with RH imprints only a portion of phytoliths, with the other portion formed from unevaporated water, then the apparent average values of $\Delta^{18}\text{O}_{\text{Phyto-LW}}$ and $\lambda_{\text{Phyto-LW}}$ will be lower than the values expected for isotope equilibrium. The magnitude of the resulting apparent fractionation will depend on the proportion of short cell phytoliths and the difference of isotope compositions between evaporated and unevaporated leaf water. The two parameters vary with RH and VPD in opposite ways. Our data show that the distance between $\Delta^{18}\text{O}_{\text{Phyto-LW}}$ and equilibrium $\Delta^{18}\text{O}_{\text{Silica-water}}$ values increases with RH, at the same time as the proportion of short cell phytoliths (inverse of LC, Table 1 and Alexandre et al., 2018) increases, suggesting that, for the experimental conditions, the proportion of short cell phytoliths has a preponderant influence.

The triple oxygen isotope compositions of the phytolith-forming water can be predicted at 40, 60 and 80% RH for the current and 2018 growth chamber experiments (Sup. mat. 1.3), using $\Delta^{18}\text{O}_{\text{Phyto-LW}}$ and $\lambda_{\text{Phyto-LW}}$ values equivalent to the $\Delta^{18}\text{O}_{\text{Silica-water}}$ and $\lambda_{\text{Silica-water}}$ expected for equilibrium (Dodd and Sharp, 2010; Sharp et al., 2016). The regression lines from the predicted isotope compositions are shown on Fig. 4. For an equilibrium $\lambda_{\text{Phyto-LW}}$ value of 0.524 the phytolith-forming water lines are far



from the leaf water ones. For a $\lambda_{\text{Phyto-LW}}$ value of 0.522, the phytolith-forming water lines are approaching the leaf water ones.
360 At 40% RH, the ^{17}O -excess of the phytolith-forming water is close to that of bulk leaf water. However, at 60 and 80 % RH the
 ^{17}O -excess of the phytolith-forming water is systematically higher than the ^{17}O -excess of bulk leaf water. At 80% RH, it is
even closer to the ^{17}O -excess of irrigation water than to that of bulk leaf water. The process described above may explain the
offsets between phytolith-forming water and bulk leaf water $\delta^{18}\text{O}$ and ^{17}O -excess values, especially pronounced at high RH.
It can also account for the low $\lambda_{\text{Phyto-LW}}$ values frequently encountered in phytolith studies. However, the imprecision of the
365 measured $\lambda_{\text{Phyto-LW}}$ values that can vary by ± 0.001 for a specific climate treatment (Sup. mat. 1.3) makes it impossible to
discern a trend of the apparent fractionation with RH or VPD.

5.3 The RH proxy

Whatever are the processes responsible for the low apparent $\lambda_{\text{Phyto-LW}}$ values, their effect on the RH-dependency of the ^{17}O -
excess of phytoliths appears weak or reproducible. This RH-dependency can be expressed for the current growth chamber
370 experiment by (eq.9)

$$^{17}\text{O-excess}_{\text{phyto}} \text{ (per meg)} = 4.1 (\pm 0.3) * \text{RH} (\%) - 500 (\pm 18) \quad (r^2 = 0.97; \text{p-value} < 0.0001), \quad (9)$$

that is indistinguishable from (eq. 10) expressed for the 2018 growth chamber experiment

$$^{17}\text{O-excess}_{\text{phyto}} \text{ (per meg)} = 4.4 (\pm 0.5) * \text{RH} (\%) - 510 (\pm 33) \quad (r^2 = 0.92; \text{p-value} < 0.001). \quad (10)$$

When applying (eq. 10) to calculate $^{17}\text{O-excess}_{\text{phyto}}$ from RH estimated for the 2018 natural transect (yearly averages of monthly
375 RH means for months with at least 1 day of precipitation higher than 0.1 mm), the mean difference is 1 ± 28 per meg (n=55).
It is 12 ± 28 per meg when using (eq. 9)

Added to the fact that the ^{17}O -excess of phytoliths is insensitive to changes in the $\delta^{18}\text{O}$ of source water, T_{air} , pCO_2 , or grass
physiognomy (Alexandre et al., 2019), this consistency between equations supports that in the 40 to 80% range, RH can be
reconstructed by (eq. 11)

$$380 \text{RH} (\%) = 0.24 \pm 0.02 * ^{17}\text{O-excess}_{\text{phyto}} \text{ (per meg)} + 121 \pm 5 \quad (r^2 = 0.98; \text{p-value} < 0.0001), \quad (11)$$

expressed for the current growth chamber experiment, and that is not different from (eq. 12)

$$\text{RH} (\%) = 0.21 \pm 0.02 * ^{17}\text{O-excess}_{\text{phyto}} \text{ (per meg)} + 112 \pm 6 \quad (r^2 = 0.92; \text{p-value} < 0.0001), \quad (12)$$

expressed for the 2018 growth chamber experiment. For both equations the statistical standard error associated with the RH
estimates is close to 3%.

385 6. Conclusions

An inter-laboratory comparison (CEREGE-UNM) allowed us to standardize the phytolith triple oxygen isotope data relative
to the VSMOW-SLAP scale. After this standardization, the apparent $\lambda_{\text{Phyto-LW}}$ values obtained so far vary between 0.521 and
0.523 \pm 0.0004 (Alexandre et al., 2018, 2019b). Heterogeneous silicification mechanisms in the leaves may result in an
apparent kinetic fractionation and explain at least partly that $\lambda_{\text{Phyto-LW}}$ values are lower than the 0.524 value expected for
390 equilibrium. When the forming water is well constrained as for phytoliths from non transpiring grass stems, the apparent $\lambda_{\text{Silica-}}$
 water value is 0.523 ± 0.0004 , i.e. close to the equilibrium value.

The datasets presented for phytoliths, leaf waters and source waters show that the $\delta^{18}\text{O}$ value of the source water governs the
position of the evaporation lines shown in the $\delta^{18}\text{O}$ vs ^{17}O -excess space for leaf water, phytoliths and phytolith-forming water.
However, since the ^{17}O -excess of the source waters varies little in growth chamber and in natural environment, the RH-
395 dependency of the ^{17}O -excess of phytoliths, verified for the 40-80% RH range, is not affected. This RH-dependency is not
impacted either by the imposed T_{air} and pCO_2 changes. The RH proxy (eq. 11) and (eq. 12) implies that each per meg of
changes in ^{17}O -excess reflects a change in RH ranging from 0.19 to 0.26 %. The ± 15 per meg reproducibility on the



measurement of the ^{17}O -excess of phytoliths corresponds to a $\pm 3.6\%$ precision on the reconstructed RH. The low sensitivity
of phytolith ^{17}O -excess to climate parameters other than relative humidity makes it particularly suitable for quantitative
400 reconstructions of continental atmospheric humidity changes in the past.

From there on, additional measurements of the triple oxygen isotope compositions of phytoliths, soil water and rainwater from
sites located under different climate and covered by different vegetation types, as well as an examination of which RH (annual
or seasonal, averaged over the growing period or over the growing period and the beginning of senescence?) is captured by
the ^{17}O -excess of phytolith assemblages extracted from sediments will help to further specify the precision and the accuracy
405 of this new RH proxy.



7. Appendices

Appendix A. Detailed description of the experimental protocol implemented in the growth chambers

Three growth chambers with a regulation of light intensity, air temperature (T_{air}), relative humidity (RH) and concentration of CO_2 (CO_2) were used to cultivate the grass *Festuca arundinacea* Schreb. in soil containers. These growth chambers had been adapted to allow for the monitoring of the isotope composition of the water compartments in the soil-plant-atmosphere continuum. In order to avoid isotope fractionation associated with water vapor condensation on the chamber walls, the chamber was flushed with $15 \text{ m}^3\text{h}^{-1}$ flow of dry air. This dry air was cooled down (or heated) to regulate the chamber T_{air} . Water vapor, produced without isotope fractionation from a reservoir of water of known isotope composition using an ultrasonic humidifier, was fogged into the chamber to reach the required RH. The humid air flow rate out of the chamber was maintained at a slightly lower value than the dry air inflow rate in order to create a slight overpressure in the chamber, preventing any outside air (and its water vapor) from entering the chamber. Pure CO_2 was injected into the chamber to reach and maintain the required CO_2 . Three plastic containers ($53 \times 35 \times 22 \text{ cm LxWxD}$) were filled with a 1.6 cm layer of quartz gravel on top of which 20 kg of dry commercial potting soil were added. A porous cup for water extraction was placed below the soil surface with its extraction tube hermetically extending outside of the container. The soil was humidified with a water of known isotope composition, also used for irrigation. The containers were sealed with a solid plastic lid to prevent soil evaporation. Twenty-four openings of $9 \times 0.8 \text{ cm}$ were cut into the lids and approximately fifty seeds of *F. arundinacea* were sown in each opening. During the germination period (from 18 to 21 days) the lids were covered with a transparent plastic film to keep a high RH around the seeds and to prevent evaporation. When most shoots reached a height of 4 cm, the plastic films were removed and silicone rubber (Bluesil™) was spread to fill-up the openings, making sure it sealed the base of all the shoots. Elasticity of the rubber allowed the stems to grow in thickness while completely preventing soil evaporation. The containers were then introduced in the growth chambers to start the experiments. The *F. arundinacea* shoots were cut at 2 cm above the container lid, so that the regrowth took place under the imposed climate conditions. In each growth chamber, the soil was continuously irrigated from a Mariotte bottle (25L) connected to the base of the container, so that a water saturation level of 5 cm was maintained at the base of the soil. Irrigation water in the Mariotte bottle was supplemented with 105 mg L^{-1} of SiO_2 (in the form of $\text{SiO}_2 \cdot \text{K}_2\text{O}$) and liquid paraffin was added on the water surface to prevent evaporation from the Mariotte bottle. The irrigation water was supplied from a large stock of ^{18}O -enriched water. The ^{18}O -enrichment was achieved by evaporation at 60°C under a flow of dry air and carried out so that the difference between the $d^{18}\text{O}$ value of irrigation water and that of fogged water was set close to the water liquid-vapor equilibrium fractionation characteristic of natural systems (e.g. $D^{18}\text{O}$ ranging from 9.65 to 9.06‰ for between 20 and 28°C ; Majoube, 1971).

After a regrowth of 11 to 26 days, the *F. arundinacea* canopy was cut at 2 cm above the lid. The harvested leaves averaged a fresh weight of $32 \pm 24 \text{ g}$. Four grams were immediately inserted into glass gastight vials for leaf water extraction and the remnant/ remaining biomass was dried at 50°C and kept for phytolith extraction. Seven combinations of RH (40, 60 and 80%), T_{air} (20, 24 and 28°C) and $p\text{CO}_2$ (200, 300 and 400 ppm) were applied to the regrowths. The light was kept constant at $100 \mu\text{mol}\cdot\text{m}^{-2}\cdot\text{s}^{-1}$ (provided by plasma lamps). For each combination, two to three replicates were run (Table 1). Due to constraints on the availability of the growth chambers, 3 to 6 regrowths were carried out successively on the same container. A failed growth, likely due to a lack of soil oxygenation, led to the preparation of a fourth container replacing one of the three initial containers. Since all the leaves of a regrowth were harvested at the end of each treatment, the interaction between the successive treatments on the same container should not affect the biomass productivity, the silicification pattern or the isotope composition of the bulk leaf water and phytoliths.

The air of each of the three growth chambers was continuously pumped via three $1/8''$ heated copper lines, at a flow rate of 0.5 l min^{-1} , and sent to a spectrometer for sequential analyses. The irrigation (Mariotte bottles), fogged (humidifier reservoir) and soil water were sampled before each regrowth and analyzed as described below. The volume of irrigation water consumed



by transpiration was estimated by measuring the volume of water in the Mariotte bottle before and after each regrowth. The volume of fogged water was estimated by doing the same with the fogged water reservoir.

450 **Appendix B. Triple oxygen isotope analyses of water laboratory standards: inter-laboratory comparison**

	CRDS -Ecotron Picarro L2140i							CRDS -CEREGE Picarro L2140i							IRMS -LSCE MAT 253			Ecotron-LSCE			Ecotron-CEREGE			CEREGE-LSCE				
	$\delta^{18}\text{O}$		$\delta^{17}\text{O}$		^{17}O -excess	n		$\delta^{18}\text{O}$		$\delta^{17}\text{O}$		^{17}O -excess	s.d.		n		$\delta^{18}\text{O}$	$\delta^{17}\text{O}$	^{17}O -excess									
	Av.	s.d.	Av.	s.d.	Av.	s.d.		Av.	s.d.	Av.	s.d.	Av.	s.d.															
‰				per meg				‰				per meg				‰			per meg			‰			per meg			
GIENS-1	-0.127	0.100	-0.066	0.060	1	7	12	-0.076	0.049	-0.039	0.019	1	11	3			-0.257	-0.141	-5	0.13	0.08	6	-0.05	-0.03	0	0.18	0.10	6
ECO-1	-5.676	0.100	-2.972	0.050	29	4	12	-5.578	0.003	-2.924	0.015	25	13	3			-5.610	-2.938	28	-0.07	-0.03	1	-0.10	-0.05	4	0.03	0.01	-3
ICEBERG-	-26.882	0.130	-14.250	0.070	36	9	12	-26.717	0.045	-14.170	0.032	27	15	3			-27.125	-14.380	35	0.24	0.13	1	-0.17	-0.08	9	0.41	0.21	-8

Table B1: Comparison between Ecotron, CEREGE and LSCE triple oxygen isotope measurements by CRDS and IRMS for three working standards of water. Av.: average; s.d.: standard deviation.

Appendix C. Triple oxygen isotope analyses of silica

455 Isotope compositions obtained from the analyses of NBS28 and seven silica working standards at CEREGE were compared to those obtained from the same standards measured at the University of New Mexico (UNM), where the reference gas is calibrated relative to VSMOW-SLAP. The working standards are UWG-2 (garnet; University of Wisconsin, Valley et al., 1995), NM-SCO (olivine; UNM), NM-Q (quartz; Wostbrock et al., 2020), CEREGE-SCO (olivine; CEREGE), Boulangé 2008 (quartz; CEREGE), MSG50-900°C and P4-40-120717-900°C (phytolith standards dehydrated under N₂ flow; CEREGE). The values are presented in Table C1. When excluding SCO that is known to be heterogeneous in $\delta^{18}\text{O}$ (Suavet et al., 2009; Wostbrock et al., 2020), the averaged CEREGE-UNM ^{17}O -excess offset is -25 per meg. The offset is independent from the $\delta^{18}\text{O}$ value of the analysed sample. Since it is larger than the data precision (15 per meg), all the silica data obtained at CEREGE were corrected by adding 20 per meg to the measured $\delta^{17}\text{O}$ value (which is equivalent to adding 20 per meg to the $\delta^{17}\text{O}$ or ^{17}O -excess values).

465

Standard	CEREGE uncorrected values										UNM values calibrated relative to VSMOW and SLAP2										CEREGE offset			CEREGE corrected values					
	$\delta^{18}\text{O}$		$\delta^{17}\text{O}$		$\delta^{18}\text{O}$	$\delta^{17}\text{O}$		^{17}O -excess	s.d.		n		$\delta^{18}\text{O}$		$\delta^{17}\text{O}$		$\delta^{18}\text{O}$	s.d.		n		$\delta^{18}\text{O}$	$\delta^{17}\text{O}$	^{17}O -excess	$\delta^{18}\text{O}$	$\delta^{17}\text{O}$	^{17}O -excess		
	Av.	s.d.	Av.	s.d.	Av.	s.d.	Av.	s.d.	Av.	s.d.		Av.	s.d.	Av.	s.d.	Av.	s.d.												
‰ vs VSMOW				per meg				‰ vs VSMOW				per meg				‰			per meg			‰ vs VSMOW			per meg				
¹ NM-	6.874	0.20	3.550	0.10	6.851	3.543	-74	3	0.517	2	5.320	0.16	2.750	0.08	5.306	2.746	-55		0.517	1.545	-19			6.874	3.570	6.851	3.563	-54	0.520
CEREGE	5.069	0.30	2.615	0.16	5.056	2.612	-58	16	0.517	4														5.069	2.635	5.056	2.632	-38	0.521
¹ UWG-2	5.716	0.12	2.950	0.07	5.700	2.945	-64	13	0.517	5	5.700		2.940	0.05	5.684	2.936	-65		0.515	0.016	1	0.001		5.716	2.970	5.700	2.965	-44	0.520
¹ NBS28	9.581	0.08	4.977	0.05	9.535	4.965	-70	15	0.521	4	9.570		4.991	0.05	9.524	4.979	-50		0.522	0.011	-20			9.581	4.997	9.535	4.984	-50	0.523
² Boulangé	16.25	0.20	8.440	0.10	16.12	8.405	-107	13	0.521	100	15.82	0.05	8.240	0.03	15.70	8.206	-84	2	0.523	0.421	-23			16.25	8.460	16.12	8.424	-88	0.523
³ NM-Q	18.04	0.21	9.374	0.10	17.88	9.330	-113	13	0.522	3	18.07	0.13	9.419	0.07	17.90	9.375	-81	5	0.523	-	-32			18.04	9.394	17.88	9.350	-93	0.523
⁴ MSG50	36.37	0.21	18.81	0.12	35.72	18.63	-226	12	0.522	2	35.57		18.44		34.95	18.27	-179	1	0.523	0.768	-46			36.37	18.83	35.72	18.65	-206	0.522
⁵ P4-40-	48.95	0.54	25.17	0.28	47.79	24.86	-367	3	0.520	2	48.45	0.81	24.95	0.41	47.32	24.64	-339	4	0.521	0.469	-28			48.95	25.19	47.79	24.88	-347	0.521
Offset standard																					0.277 -25 -			0.325 16 0.001					

¹Sharp and Wostbrock, 2021

²measured at UNM for the present study

³Wostbrock et al., 2020

470 **Table C1: Comparison between the triple oxygen isotope compositions of silica standards analyzed at CEREGE and the University of New Mexico. s.d.: standard deviation.**

475 It was recently suggested that when analyzing biogenic silica, the methods used for dehydration may bias the measured ^{17}O -excess values (Herwartz, 2021). This should affect also the $\delta^{18}\text{O}$ value. It was indeed experimentally shown long ago that simple dehydroxylation at high temperature modifies the $\delta^{18}\text{O}$ value of hydrous silica. This was explained by incomplete removal of the exchangeable oxygens included in silanol groups, that get trapped in the silica structure when new siloxane



groups form at high temperature (Labeyrie and Juillet, 1982). Based on this observation, several methods have been developed to fix the isotope composition of the exchangeable oxygen by isotope equilibration (Leclerc and Labeyrie, 1987) or remove all the exchangeable oxygen by stepwise fluorination (Chapligin et al., 2010; Haimson and Knauth, 1983; Leclerc and Labeyrie, 1987). An inter-laboratory comparison showed that there is a good agreement between the $\delta^{18}\text{O}$ values obtained
480 from these different methods (Chapligin et al., 2011). The dehydroxylation under N_2 flow used today at CEREGE leads to $\delta^{18}\text{O}$ values for the biogenic working standards BFC (NERC), PS1772-8 (AWI) and MSG60 (CEREGE) of $28.3 \pm 0.6\text{‰}$ ($n = 7$), $43.0 \pm 0.3\text{‰}$ ($n = 6$) and $37.5 \pm 0.3\text{‰}$ ($n = 2$), respectively, in agreement with the inter-laboratory comparison pooled values ($29.0 \pm 0.3\text{‰}$, $42.8 \pm 0.8\text{‰}$ and $37.0 \pm 0.8\text{‰}$, respectively). The breaking of siloxane groups during the heating stage was also put forward as a process that could induce an isotope bias (Herwartz, 2021). In order to examine this assumption, the NBS28
485 quartz standard was analyzed at CEREGE after being heated at 900°C under a N_2 flow. The aliquots processed in this way gave the same $\delta^{18}\text{O}$ and ^{17}O -excess values ($9.727 \pm 0.227\text{‰}$ and -51 ± 12 per meg ($n = 7$) for $\delta^{18}\text{O}$ and ^{17}O -excess, respectively) as the unprocessed aliquots ($9.581 \pm 0.080\text{‰}$ and -50 ± 15 per meg ($n = 4$), for $\delta^{18}\text{O}$ and ^{17}O -excess, respectively). These data argue for the absence of significant isotope fractionation during the biogenic silica dehydration step.

9. Supplement link

490 10. Author contribution

C. Outrequin and A. Alexandre wrote the initial draft. A. Alexandre, C. Outrequin, J. Roy, A. Landais, C. Piel, S. Devidal, C. Vallet-Coulomb, C. Peugeot and C. Voigt participated to the writing and editing of the final draft. C. Piel, S. Devidal, J. Roy, A. Alexandre, C. Vallet-Coulomb and A. Landais conceptualized the growth chamber experiment and designed the methodology. C. Outrequin, C. Piel, S. Devidal and A. Alexandre conducted the growth chamber experiment. A. Alexandre,
495 C. Outrequin, C. Vallet Coulomb and C. Peugeot designed and conducted the experiment at the AMMA-CATCH site. C. Piel, A. Alexandre, C. Outrequin, A. Landais, C. Vallet-Coulomb, C. Sonzogni, M. Couapel, M. Pierre, F. Prié, and J.C. Mazur performed the analyses. A. Alexandre acquired the funding, managed and supervised the project.

11. Competing interests

The authors declare that they have no conflict of interest

500 12. Acknowledgements

The authors express their gratitude to Zachary Sharp, for the isotope measurements of the silica laboratory standards at the University of New Mexico. The authors also thank Theodore Ouani, Simon Afouda and Maxime Wubda (IRD-Benin) for their essential contribution at the AMMA-CATCH observatory. Our research was conducted in the frame of the HUMI-17 project supported by INSU-LEFE, the ANR (grant nos. ANR-17-CE01-0002-01), ECCOREV and labex OT-Med. It benefited from
505 the CNRS human and technical resources allocated to the Ecotrons Research Infrastructure from the state allocation 'Investissement d'Avenir' AnaEEFrance ANR-11-INBS-0001.

13. References

Ainsworth, E. A. and Rogers, A.: The response of photosynthesis and stomatal conductance to rising $[\text{CO}_2]$: mechanisms and environmental interactions, *Plant Cell Environ.*, 30, 258–270, <https://doi.org/10.1111/j.1365-3040.2007.01641.x>, 2007.
510 Alexandre, A., Basile-Doelsch, I., Sonzogni, C., Sylvestre, F., Parron, C., Meunier, J.-D., and Colin, F.: Oxygen isotope



- analyses of fine silica grains using laser-extraction technique: Comparison with oxygen isotope data obtained from ion microprobe analyses and application to quartzite and silcrete cement investigation, *Geochimica et Cosmochimica Acta*, 70, 2827–2835, <https://doi.org/10.1016/j.gca.2006.03.003>, 2006.
- Alexandre, A., Crespin, J., Sylvestre, F., Sonzogni, C., and Hilbert, D. W.: The oxygen isotopic composition of phytolith assemblages from tropical rainforest soil tops (Queensland, Australia): validation of a new paleoenvironmental tool, 8, 307–324, 2012.
- Alexandre, A., Landais, A., Vallet-Coulomb, C., Piel, C., Devidal, S., Pauchet, S., Sonzogni, C., Couapel, M., Pasturel, M., Cornuault, P., Xin, J., Mazur, J.-C., Prié, F., Bentaleb, I., Webb, E., Chalié, F., and Roy, J.: The triple oxygen isotope composition of phytoliths as a proxy of continental atmospheric humidity: insights from climate chamber and climate transect calibrations, *Biogeosciences*, 15, 3223–3241, <https://doi.org/10.5194/bg-15-3223-2018>, 2018.
- Alexandre, A., Webb, E., Landais, A., Piel, C., Devidal, S., Sonzogni, C., Couapel, M., Mazur, J.-C., Pierre, M., Prié, F., Vallet-Coulomb, C., and Roy, J.: Effects of grass leaf anatomy, development and light/dark alternation on the triple oxygen isotope signature of leaf water and phytoliths: insights for a new proxy of continental atmospheric humidity, 1–17, <https://doi.org/10.5194/bg-2019-73>, 2019a.
- Alexandre, A., Webb, E., Landais, A., Piel, C., Devidal, S., Sonzogni, C., Couapel, M., Mazur, J.-C., Pierre, M., Prié, F., Vallet-Coulomb, C., Outrequin, C., and Roy, J.: Effects of leaf length and development stage on the triple oxygen isotope signature of grass leaf water and phytoliths: insights for a proxy of continental atmospheric humidity, 16, 4613–4625, <https://doi.org/10.5194/bg-16-4613-2019>, 2019b.
- Angert, A., Rachmilevitch, S., Barkan, E., and Luz, B.: Effects of photorespiration, the cytochrome pathway, and the alternative pathway on the triple isotopic composition of atmospheric O₂, *Global Biogeochem. Cycles*, 17, 1030, <https://doi.org/10.1029/2002GB001933>, 2003.
- Aron, P. G., Levin, N. E., Beverly, E. J., Huth, T. E., Passey, B. H., Pelletier, E. M., Poulsen, C. J., Winkelstern, I. Z., and Yarian, D. A.: Triple oxygen isotopes in the water cycle, *Chemical Geology*, 120026, <https://doi.org/10.1016/j.chemgeo.2020.120026>, 2020.
- Barillot, R., Frak, E., Combes, D., Durand, J.-L., and Escobar-Gutiérrez, A. J.: What determines the complex kinetics of stomatal conductance under blueless PAR in *Festuca arundinacea*? Subsequent effects on leaf transpiration, *J. Exp. Bot.*, 61, 2795–2806, <https://doi.org/10.1093/jxb/erq115>, 2010.
- Barkan, E. and Luz, B.: High precision measurements of ¹⁷O/¹⁶O and ¹⁸O/¹⁶O ratios in H₂O, *Rapid Commun. Mass Spectrom.*, 19, 3737–3742, <https://doi.org/10.1002/rcm.2250>, 2005.
- Barkan, E. and Luz, B.: Diffusivity fractionations of H₂(¹⁶O)/H₂(¹⁷O) and H₂(¹⁶O)/H₂(¹⁸O) in air and their implications for isotope hydrology, *Rapid Commun. Mass Spectrom.*, 21, 2999–3005, <https://doi.org/10.1002/rcm.3180>, 2007.
- Blunier, T., Barnett, B., Bender, M. L., and Hendricks, M. B.: Biological oxygen productivity during the last 60,000 years from triple oxygen isotope measurements, *Global Biogeochem. Cycles*, 16, 3–1, <https://doi.org/10.1029/2001GB001460>, 2002.
- Bony, S., Colman, R., Kattsov, V. M., Allan, R. P., Bretherton, C. S., Dufresne, J.-L., Hall, A., Hallegatte, S., Holland, M. M., Ingram, W., Randall, D. A., Soden, B. J., Tselioudis, G., and Webb, M. J.: How Well Do We Understand and Evaluate Climate Change Feedback Processes?, *J. Climate*, 19, 3445–3482, <https://doi.org/10.1175/JCLI3819.1>, 2006.
- Bowen, G. J., Wassenaar, L. I., and Hobson, K. A.: Global application of stable hydrogen and oxygen isotopes to wildlife forensics, *Oecologia*, 143, 337–348, <https://doi.org/10.1007/s00442-004-1813-y>, 2005.
- Brandon, M., Landais, A., Duchamp-Alphonse, S., Favre, V., Schmitz, L., Abrial, H., Prié, F., Extier, T., and Blunier, T.: Exceptionally high biosphere productivity at the beginning of Marine Isotopic Stage 11, 11, 2112, <https://doi.org/10.1038/s41467-020-15739-2>, 2020.
- Cao, X. and Liu, Y.: Equilibrium mass-dependent fractionation relationships for triple oxygen isotopes, *Geochimica et*



- Cosmochimica Acta, 75, 7435–7445, <https://doi.org/10.1016/j.gca.2011.09.048>, 2011.
- 555 Cernusak, L. A., Barbour, M. M., Arndt, S. K., Cheesman, A. W., English, N. B., Feild, T. S., Helliker, B. R., Holloway-Phillips, M. M., Holtum, J. A. M., Kahmen, A., McInerney, F. A., Munksgaard, N. C., Simonin, K. A., Song, X., Stuart-Williams, H., West, J. B., and Farquhar, G. D.: Stable isotopes in leaf water of terrestrial plants, *Plant, Cell & Environment*, 39, 1087–1102, <https://doi.org/10.1111/pce.12703>, 2016.
- Chapligin, B., Meyer, H., Friedrichsen, H., Marent, A., Sohns, E., and Hubberten, H.-W.: A high-performance, safer and semi-automated approach for the delta18O analysis of diatom silica and new methods for removing exchangeable oxygen, *Rapid Commun. Mass Spectrom.*, 24, 2655–2664, <https://doi.org/10.1002/rcm.4689>, 2010.
- 560 Chapligin, B., Leng, M. J., Webb, E., Alexandre, A., Dodd, J. P., Ijiri, A., Lücke, A., Shemesh, A., Abelmann, A., Herzschuh, U., Longstaffe, F. J., Meyer, H., Moschen, R., Okazaki, Y., Rees, N. H., Sharp, Z. D., Sloane, H. J., Sonzogni, C., Swann, G. E. A., Sylvestre, F., Tyler, J. J., and Yam, R.: Inter-laboratory comparison of oxygen isotope compositions from biogenic silica, 75, 7242–7256, 2011.
- 565 Chung, E.-S., Soden, B., Sohn, B. J., and Shi, L.: Upper-tropospheric moistening in response to anthropogenic warming, *PNAS*, 111, 11636–11641, <https://doi.org/10.1073/pnas.1409659111>, 2014.
- Corbineau, R., Reyerson, P. E., Alexandre, A., and Santos, G. M.: Towards producing pure phytolith concentrates from plants that are suitable for carbon isotopic analysis, *Review of Palaeobotany and Palynology*, 197, 179–185, <https://doi.org/10.1016/j.revpalbo.2013.06.001>, 2013.
- 570 Craig, H. and Gordon, L. I.: Deuterium and Oxygen 18 Variations in the Ocean and the Marine Atmosphere, *Consiglio nazionale delle ricerche, Laboratorio de geologia nucleare*, 128 pp., 1965.
- Crespin, J., Alexandre, A., Sylvestre, F., Sonzogni, C., Paillès, C., and Garreta, V.: IR laser extraction technique applied to oxygen isotope analysis of small biogenic silica samples, *Anal. Chem.*, 80, 2372–2378, <https://doi.org/10.1021/ac071475c>, 2008.
- 575 Dessler, A. E. and Davis, S. M.: Trends in tropospheric humidity from reanalysis systems, *J. Geophys. Res.*, 115, D19127, <https://doi.org/10.1029/2010JD014192>, 2010.
- Dodd, J. P. and Sharp, Z. D.: A laser fluorination method for oxygen isotope analysis of biogenic silica and a new oxygen isotope calibration of modern diatoms in freshwater environments, *Geochimica et Cosmochimica Acta*, 74, 1381–1390, <https://doi.org/10.1016/j.gca.2009.11.023>, 2010.
- 580 Extier, T., Landais, A., Bréant, C., Prié, F., Bazin, L., Dreyfus, G., Roche, D. M., and Leuenberger, M.: On the use of $\delta^{18}\text{O}_{\text{atm}}$ for ice core dating, *Quaternary Science Reviews*, 185, 244–257, <https://doi.org/10.1016/j.quascirev.2018.02.008>, 2018.
- Farquhar, G. D. and Gan, K. S.: On the progressive enrichment of the oxygen isotopic composition of water along a leaf, *Plant Cell Environ.*, 26, 801–819, 2003.
- 585 Farquhar, G. D. and Lloyd, J.: 5 - Carbon and Oxygen Isotope Effects in the Exchange of Carbon Dioxide between Terrestrial Plants and the Atmosphere, in: *Stable Isotopes and Plant Carbon-water Relations*, edited by: Ehleringer, J. R., Hall, A. E., and Farquhar, G. D., Academic Press, San Diego, 47–70, <https://doi.org/10.1016/B978-0-08-091801-3.50011-8>, 1993.
- Farquhar, G. D., Cernusak, L. A., and Barnes, B.: Heavy Water Fractionation during Transpiration, *Plant Physiol*, 143, 11–18, <https://doi.org/10.1104/pp.106.093278>, 2007.
- 590 Galle, S., Grippa, M., Peugeot, C., Moussa, I. B., Cappelaere, B., Demarty, J., Mougín, E., Panthou, G., Adjomayi, P., Agbossou, E. K., Ba, A., Boucher, M., Cohard, J.-M., Descloitres, M., Descroix, L., Diawara, M., Dossou, M., Favreau, G., Gangneron, F., Gosset, M., Hector, B., Hiernaux, P., Issoufou, B.-A., Kergoat, L., Lawin, E., Lebel, T., Legchenko, A., Abdou, M. M., Malam-Issa, O., Mamadou, O., Nazoumou, Y., Pellarin, T., Quantin, G., Sambou, B., Seghieri, J., Séguis, L., Vandervaere, J.-P., Vischel, T., Vouillamoz, J.-M., Zannou, A., Afouda, S., Alhassane, A., Arjounin, M., Barral, H., Biron, R., Cazenave, F., Chaffard, V., Chazarin, J.-P., Guyard, H., Koné, A., Mainassara, I., Mamane, A., Oi, M., Ouani, T., Soumaguel, N., Wubda, M., Ago, E. E., Alle, I. C., Allies, A., Arpin-Pont, F., Awessou, B., Cassé, C., Charvet, G., Dardel,
- 595



- C., Depeyre, A., Diallo, F. B., Do, T., Fatras, C., Frappart, F., Gal, L., Gascon, T., Gibon, F., Guiro, I., Ingatan, A., Kempf, J., Kotchoni, D. O. V., Lawson, F. M. A., Leauthaud, C., Louvet, S., Mason, E., Nguyen, C. C., Perrimond, B., Pierre, C., Richard, A., Robert, E., Román-Cascón, C., Velluet, C., and Wilcox, C.: AMMA-CATCH, a Critical Zone Observatory in West Africa
600 Monitoring a Region in Transition, 17, 180062, <https://doi.org/10.2136/vzj2018.03.0062>, 2018.
- Gan, K. S., Wong, S. C., Yong, J. W. H., and Farquhar, G. D.: Evaluation of models of leaf water ^{18}O enrichment using measurements of spatial patterns of vein xylem water, leaf water and dry matter in maize leaves, 26, 1479–1495, <https://doi.org/10.1046/j.1365-3040.2003.01070.x>, 2003.
- Garcin, Y., Schwab, V. F., Gleixner, G., Kahmen, A., Todou, G., Séné, O., Onana, J.-M., Achoundong, G., and Sachse, D.:
605 Hydrogen isotope ratios of lacustrine sedimentary n-alkanes as proxies of tropical African hydrology: Insights from a calibration transect across Cameroon, *Geochimica et Cosmochimica Acta*, 79, 106–126, <https://doi.org/10.1016/j.gca.2011.11.039>, 2012.
- Gat, J. R.: Oxygen and Hydrogen Isotopes in the Hydrologic Cycle, 24, 225–262, <https://doi.org/10.1146/annurev.earth.24.1.225>, 1996.
- 610 Gibson, D. J. and Newman, J. A.: *Festuca arundinacea* Schreber (*F. elatior* L. ssp. *arundinacea* (Schreber) Hackel), 89, 304–324, <https://doi.org/10.1046/j.1365-2745.2001.00561.x>, 2001.
- Govin, A., Varma, V., and Prange, M.: Astronomically forced variations in western African rainfall (21°N – 20°S) during the Last Interglacial period, 41, 2117–2125, <https://doi.org/10.1002/2013GL058999>, 2014.
- Haimson, M. and Knauth, L. P.: Stepwise fluorination - a useful approach for the isotopic analysis of hydrous minerals, 47:9,
615 [https://doi.org/10.1016/0016-7037\(83\)90185-0](https://doi.org/10.1016/0016-7037(83)90185-0), 1983.
- Held, I. M. and Soden, B. J.: Water Vapor Feedback and Global Warming, 25, 441–475, <https://doi.org/10.1146/annurev.energy.25.1.441>, 2000.
- Herwartz, D.: Triple Oxygen Isotope Variations in Earth’s Crust, *Reviews in Mineralogy and Geochemistry*, 86, 291–322, <https://doi.org/10.2138/rmg.2021.86.09>, 2021.
- 620 Hirl, R. T., Schnyder, H., Ostler, U., Schäufele, R., Schleip, I., Vetter, S. H., Auerswald, K., Baca Cabrera, J. C., Wingate, L., Barbour, M. M., and Ogée, J.: The ^{18}O ecohydrology of a grassland ecosystem – predictions and observations, 23, 2581–2600, <https://doi.org/10.5194/hess-23-2581-2019>, 2019.
- Hofmann, M. E. G., Horvath, B., Schneider, L., Peters, W., Schützenmeister, K., and Pack, A.: Atmospheric measurements of $\Delta 17\text{O}$ in CO_2 in Göttingen, Germany reveal a seasonal cycle driven by biospheric uptake, 199, 143–163,
625 <https://doi.org/10.1016/j.gca.2016.11.019>, 2017.
- IPCC Staff.: Climate Change (2007) Synthesis Report. Contribution of Working Groups I, II and III to the Fourth Assessment Report of the Intergovernmental Panel on Climate Change., 2007.
- Koren, G., Schneider, L., van der Velde, I. R., van Schaik, E., Gromov, S. S., Adnew, G. A., Mrozek Martino, D. J., Hofmann, M. E. G., Liang, M.-C., Mahata, S., Bergamaschi, P., van der Laan-Luijkx, I. T., Krol, M. C., Röckmann, T., and Peters, W.:
630 Global 3-D Simulations of the Triple Oxygen Isotope Signature $\Delta 17\text{O}$ in Atmospheric CO_2 , *Journal of Geophysical Research: Atmospheres*, 124, 8808–8836, <https://doi.org/10.1029/2019JD030387>, 2019.
- Kumar, S., Soukup, M., and Elbaum, R.: Silicification in Grasses: Variation between Different Cell Types, *Front. Plant Sci.*, 8, <https://doi.org/10.3389/fpls.2017.00438>, 2017.
- Labeyrie, L. and Juillet, A.: Oxygen isotopic exchangeability of diatom valve silica; interpretations and consequences for paleoclimatic studies, *Geochim. Cosmochim. Acta*, 46, 967–975, 1982.
- 635 Landais, A., Barkan, E., and Luz, B.: Record of $\delta 18\text{O}$ and ^{17}O -excess in ice from Vostok Antarctica during the last 150,000 years, *Geophys. Res. Lett.*, 35, L02709, <https://doi.org/10.1029/2007GL032096>, 2008.
- Leaney, F. W., Osmond, C. B., Allison, G. B., and Ziegler, H.: Hydrogen-isotope composition of leaf water in C3 and C4 plants: its relationship to the hydrogen-isotope composition of dry matter, *Planta*, 164, 215–220,



- 640 <https://doi.org/10.1007/BF00396084>, 1985.
Leclerc, A. J. and Labeyrie, L.: Temperature dependence of the oxygen isotopic fractionation between diatom silica and water, *Earth and Planetary Science Letters*, 84, 69–74, [https://doi.org/10.1016/0012-821X\(87\)90177-4](https://doi.org/10.1016/0012-821X(87)90177-4), 1987.
Li, S., Levin, N. E., Soderberg, K., Dennis, K. J., and Caylor, K. K.: Triple oxygen isotope composition of leaf waters in Mpala, central Kenya, *Earth and Planetary Science Letters*, 468, 38–50, <https://doi.org/10.1016/j.epsl.2017.02.015>, 2017.
- 645 Luz, B. and Barkan, E.: Variations of $^{17}\text{O}/^{16}\text{O}$ and $^{18}\text{O}/^{16}\text{O}$ in meteoric waters, *Geochimica et Cosmochimica Acta*, 74, 6276–6286, <https://doi.org/10.1016/j.gca.2010.08.016>, 2010.
Luz, B., Barkan, E., Bender, M. L., Thiemens, M. H., and Boering, K. A.: Triple-isotope composition of atmospheric oxygen as a tracer of biosphere productivity, *Nature*, 400, 547–550, <https://doi.org/10.1038/22987>, 1999.
Majoube, M.: Fractionnement en oxygène 18 et en deutérium entre l’eau et sa vapeur, *J. Chim. Phys.*, 68, 1423–1436, <https://doi.org/10.1051/jcp/1971681423>, 1971.
- 650 Rach, O., Kahmen, A., Brauer, A., and Sachse, D.: A dual-biomarker approach for quantification of changes in relative humidity from sedimentary lipid DH ratios, *Clim. Past*, 13, 741–757, <https://doi.org/10.5194/cp-13-741-2017>, 2017.
Sachse, D., Billault, I., Bowen, G. J., Chikaraishi, Y., Dawson, T. E., Feakins, S. J., Freeman, K. H., Magill, C. R., McNerney, F. A., Van der Meer, M. T., and others: Molecular paleohydrology: interpreting the hydrogen-isotopic composition of lipid biomarkers from photosynthesizing organisms, 2012.
Schwab, V. F., Garcin, Y., Sachse, D., Todou, G., Séné, O., Onana, J.-M., Achoundong, G., and Gleixner, G.: Effect of aridity on $\delta^{13}\text{C}$ and δD values of C_3 plant- and C_4 graminoid-derived leaf wax lipids from soils along an environmental gradient in Cameroon (Western Central Africa), *Organic Geochemistry*, 78, 99–109, <https://doi.org/10.1016/j.orggeochem.2014.09.007>, 2015.
- 660 Sharp, Z. D. and Wostbrock, J. A. G.: Standardization for the Triple Oxygen Isotope System: Waters, Silicates, Carbonates, Air, and Sulfates, *Reviews in Mineralogy and Geochemistry*, 86, 179–196, <https://doi.org/10.2138/rmg.2021.86.05>, 2021.
Sharp, Z. D., Gibbons, J. A., Maltsev, O., Atudorei, V., Pack, A., Sengupta, S., Shock, E. L., and Knauth, L. P.: A calibration of the triple oxygen isotope fractionation in the $\text{SiO}_2\text{--H}_2\text{O}$ system and applications to natural samples, 186, 105–119, <https://doi.org/10.1016/j.gca.2016.04.047>, 2016.
- 665 Sharp, Z. D., Wostbrock, J. A. G., and Pack, A.: Mass-dependent triple oxygen isotope variations in terrestrial materials, 27–31, <https://doi.org/10.7185/geochemlet.1815>, 2018.
Stevens, B., Brogniez, H., Kiemle, C., Lacour, J.-L., Crevoisier, C., and Kiliani, J.: Structure and dynamical influence of water vapor in the lower tropical troposphere, 38, 1371–1397, <https://doi.org/10.1007/s10712-017-9420-8>, 2017.
Suavet, C., Alexandre, A., Franchi, I. A., Gattacceca, J., Sonzogni, C., Greenwood, R. C., Folco, L., and Rochette, P.: Solving the parent bodies of micrometeorites with high-precision oxygen isotope ratios, 44, A197–A197, 2009.
- 670 Suavet, C., Alexandre, A., Franchi, I. A., Gattacceca, J., Sonzogni, C., Greenwood, R. C., Folco, L., and Rochette, P.: Identification of the parent bodies of micrometeorites with high-precision oxygen isotope ratios, *Earth and Planetary Science Letters*, 293, 313–320, <https://doi.org/10.1016/j.epsl.2010.02.046>, 2010.
Surma, J., Assonov, S., and Staubwasser, M.: Triple Oxygen Isotope Systematics in the Hydrologic Cycle, *Reviews in Mineralogy and Geochemistry*, 86, 401–428, <https://doi.org/10.2138/rmg.2021.86.12>, 2021.
- 675 Tuthorn, M., Zech, R., Ruppenthal, M., Oelmann, Y., Kahmen, A., del Valle, H. F., Eglinton, T., Rozanski, K., and Zech, M.: Coupling $\delta^2\text{H}$ and $\delta^{18}\text{O}$ biomarker results yields information on relative humidity and isotopic composition of precipitation – a climate transect validation study, *Biogeosciences*, 12, 3913–3924, <https://doi.org/10.5194/bg-12-3913-2015>, 2015.
Uemura, R., Barkan, E., Abe, O., and Luz, B.: Triple isotope composition of oxygen in atmospheric water vapor, *Geophys. Res. Lett.*, 37, L04402, <https://doi.org/10.1029/2009GL041960>, 2010.
- 680 Valley, J. W., Kitchen, N., Kohn, M. J., Niendorf, C. R., and Spicuzza, M. J.: UWG-2, a garnet standard for oxygen isotope ratios: Strategies for high precision and accuracy with laser heating, 59, 5223–5231, 1995.



- Webb, E. A. and Longstaffe, F. J.: The relationship between phytolith- and plant-water delta O-18 values in grasses, 67, 1437–1449, [https://doi.org/10.1016/s0016-7037\(02\)01300-5](https://doi.org/10.1016/s0016-7037(02)01300-5), 2003.
- 685 Webb, E. A. and Longstaffe, F. J.: Identifying the δ 18O signature of precipitation in grass cellulose and phytoliths: Refining the paleoclimate model, *Geochimica et Cosmochimica Acta*, 70, 2417–2426, <https://doi.org/10.1016/j.gca.2006.02.024>, 2006.
- Welp, L. R., Lee, X., Kim, K., Griffis, T. J., Billmark, K. A., and Baker, J. M.: δ 18O of water vapour, evapotranspiration and the sites of leaf water evaporation in a soybean canopy, 31, 1214–1228, <https://doi.org/10.1111/j.1365-3040.2008.01826.x>, 2008.
- 690 Wostbrock, J. A. G., Cano, E. J., and Sharp, Z. D.: An internally consistent triple oxygen isotope calibration of standards for silicates, carbonates and air relative to VSMOW2 and SLAP2, *Chemical Geology*, 533, 119432, <https://doi.org/10.1016/j.chemgeo.2019.119432>, 2020.



695 **Table 1 : The growth chamber experiment: three relative humidity (RH), air temperature (T_{air}) and CO_2 concentration (CO_2) treatments (seven climate combinations and 2 to 3 replicates per combination), *F. arundinaceae* regrowth duration, harvest fresh weight, productivity, phytolith concentration and percentage of Long cell phytolith types relative to Long and Short cell phytolith types (LC). Av. : average; s.d. : standard deviation.**

Treatments	¹ Sample	Chamber		RH	T_{min} °C	T_{leaf} °C	P_{CO_2} ppm	VPD kPa	Regrowth duration days	Harvest fresh weight g	Productivity g/day	Phytolith concentration		³ LC %		
		#	#									% d.w.	s.d.			
RH	40	2	2	40.1	24.0	22.0	400	1.78	20	32.8	1.6	3.94				
		3	3	40.2	24.0	22.0	400	1.77	20	21.1	1.1	3.23				
		4	4	40.0	24.0	22.0	400	1.78	20	34.4	1.7	1.5	0.4	31		
		2	2	59.5	24.0	22.0	400	1.20	14	15.1	1.1		4.74			
60	60	3	3	59.8	24.0	22.0	400	1.19	14	18.5	1.3	2.57		26		
		4	4	59.5	24.0	22.0	400	1.20	14	14.2	1.0	1.1	0.2	5.94	4.4	1.7
		2	2	79.1	24.0	22.0	400	0.62	26	108.4	4.2		1.74			
		3	3	79.0	24.0	22.0	400	0.62	26	75.0	2.9	3.5	0.9	1.14	1.4	0.4
T_{air}	20	3	3	60.1	20.0	18.0	400	0.93	14	25.7	1.8	2.41				
		4	4	60.1	20.0	18.0	399	0.93	14	38.4	2.7	2.3	0.6	0.80	1.6	1.1
		3	3	59.0	28.0	26.0	400	1.54	11	44.0	4.0		3.18			
		4	4	59.3	28.0	26.0	400	1.53	11	20.2	1.8		1.59			
28	28	2	5	57.9	27.8	25.8	400	1.56	14	18.0	1.3	2.4	1.4	2.57	2.4	0.8
		3	3	60.1	24.0	22.0	200	1.18	14	15.7	1.1		2.42			
		4	4	59.1	24.0	22.0	201	1.21	14	37.0	2.6	1.9	1.1	1.89	2.2	0.4
		3	3	60.0	24.0	22.0	300	1.19	14	17.7	1.3		3.19			
300	300	4	4	58.9	24.0	22.0	300	1.22	14	31.5	2.3	2.53				
		2	5	58.5	24.0	22.0	300	1.23	15	20.5	1.4	1.6	0.5	1.90	2.5	0.6

¹Sample name includes the sampling date (with DD.MM.YY)

²Long Cell phytoliths / Long and Short Cell phytoliths



Table 2 : Triple oxygen isotope fractionation observed between bulk leaf water and irrigation water and phytolith and bulk leaf water of *F. arundinaceae* for the three relative humidity (RH), air temperature (T_{air}) and CO₂ concentration (CO₂) treatments. Av.: average; s.d.: standard deviation.

Treatment	Sample	RH %	T_{sam} °C	T_{leaf} °C	P_{CO_2} ppm	VPD kPa	Apparent fractionation between irrigation (IW) and leaf water (LW)				Apparent fractionation between bulk leaf water (LW) and phytolith (Phyto)				$\lambda_{Phyto-LW}$		
							$\Delta^{18}O_{LW/IW}$ ‰		$\Delta^{17}O_{LW/IW}$ ‰		$\Delta^{18}O_{Phyto-LW}$ ‰		$\Delta^{17}O_{Phyto-LW}$ ‰			$^{17}O_{excess}$ Phyto-LW per meg	
							Av	sd	Av	sd	Av	sd	Av	sd		Av	sd
40	P2-40-12.07.17	40.1	24.0	22.0	400	1.78	9.84	5.02	0.510	33.60	17.53	-209	0.522				
	P3-40-12.07.17	40.2	24.0	22.0	400	1.77	9.53	4.86	0.510	32.23	16.85	-168	0.523				
	P4-40-12.07.17	40.0	24.0	22.0	400	1.78	10.58	9.99	0.512	30.25	32.03	1.68	0.521				
	P2-60-12.06.17	59.5	24.0	22.0	400	1.20	6.60	3.35	0.508	26.38	13.77	-163	0.522				
60	P3-60-12.06.17	59.8	24.0	22.0	400	1.19	7.35	3.75	0.510	27.04	14.12	-152	0.522				
	P4-60-12.06.17	59.5	24.0	22.0	400	1.20	7.18	7.04	0.512	26.90	26.77	0.35	0.521				
	P2-80-07.08.17	79.1	24.0	22.0	400	0.62	2.71	1.37	0.506	26.60	13.90	-149	0.522				
	P3-80-07.08.17	79.0	24.0	22.0	400	0.62	5.68	4.19	2.10	23.94	25.27	1.88	0.522				
20	P3-20-400-14.02.18	60.1	20.0	18.0	400	0.93	11.49	5.97	0.520	22.59	11.74	-188	0.520				
	P4-20-400-14.02.18	60.1	20.0	18.0	399	0.93	10.61	11.05	0.62	24.59	23.59	1.42	0.521				
	P3-28-400-10.04.18	59.0	28.0	26.0	400	1.54	6.16	3.14	0.510	26.28	13.71	-168	0.522				
	P4-28-400-10.04.18	59.3	28.0	26.0	400	1.53	6.69	3.43	0.513	26.62	13.89	-169	0.522				
28	P5-28-400-05.07.18	57.9	27.8	25.8	400	1.56	5.10	5.99	0.81	27.08	26.66	0.40	0.523				
	P3-24-200-16.03.18	60.1	24.0	22.0	200	1.18	8.19	4.21	0.514	25.46	13.29	-148	0.522				
	P4-24-200-16.03.18	59.1	24.0	22.0	201	1.21	8.63	8.41	0.32	26.25	25.85	0.56	0.522				
	P3-24-300-30.03.18	60.0	24.0	22.0	300	1.19	6.46	3.30	0.511	26.47	13.82	-157	0.522				
300	P4-24-300-30.03.18	58.9	24.0	22.0	300	1.22	10.03	5.18	0.517	24.13	12.60	-143	0.522				
	P5-24-300-10.08.18	58.5	24.0	22.0	300	1.23	7.80	8.10	1.80	26.35	25.65	1.32	0.522				
	² 60% RH Av.		7.38						0.511	26.23	13.70		0.522				
			1.10						0.003	0.56	0.29		0.0005				

¹Sample name includes the sampling date (with DD/MM/YY)
²Average and standard deviation calculated for all experiments conducted at 60% RH



705 **Table 3: $\delta^{18}\text{O}$ and ^{17}O -excess values of stem phytoliths extracted from two grass species collected at the beginning and in the middle of the rainy season, at the AMMA-CATCH natural observatory in Benin (Djougou, stations of Naholou, 9.74281 °N; 1.60635 °E and Bellefougou, 9.78992 °N, 1.71007° E). Averaged values of $\delta^{18}\text{O}$ and ^{17}O -excess for the rainwater of the rainy period preceding the samplings and values of fractionation between rainwater and phytoliths are shown. For comparison, values of fractionation between water and silica estimated according to Sharp et al. (2016) and Dodd and Sharp (2010) and assuming different values for $\lambda_{\text{silica-water}}$ are presented. Av.: average; s.d.: standard deviation.**

¹⁵ Sample	Vegetation	RH	T _{air}	T _{stem}	Phytolith (Phyto)				² Rainwater average (RW)				Observed Phyto-RW						Estimated Silica-water							
					$\delta^{18}\text{O}$		^{17}O -excess		$\delta^{18}\text{O}$		^{17}O -excess		$\Delta^{17}\text{O}$		$\Delta^{17}\text{O}$		λ		$\lambda_{\text{silica-water}}$		$\lambda_{\text{silica-water}}$		$\lambda_{\text{silica-water}}$		$\lambda_{\text{silica-water}}$	
					Av	sd	Av	sd	Av	sd	Av	sd	Av	sd	Av	sd	Av	sd	Av	sd	Av	sd	Av	sd	Av	sd
NA-Hyp-T-17.09.18	Savanna	60	25	23	26.57	0.07	13.90	0.04	-132	1	2	-4.31	-2.25	24	30.88	16.15	-156	0.523	0.523	36.98	-148	31.12	-124	-156	-187	-218
BE-Andro-T-19.09.18	Dry forest	60	25	23	27.78	0.25	14.52	0.15	-150	18	2	-4.31	-2.25	24	32.09	16.77	-174	0.523	0.523	36.98	-148	31.12	-124	-156	-187	-218
NA-Hyp-T-19.05.19	Savanna	59.8	28.3	26.3	29.18	0.45	15.24	0.23	-171	10	2	-1.94	-1.01	13	31.11	16.24	-184	0.522	0.522	36.04	-144	30.53	-122	-153	-183	-214
BE-Andro-T-20.05.19	Dry forest	61.3	29.3	27.3	28.72	0.08	15.02	0.04	-138	1	2	-1.94	-1.01	13	30.65	16.03	-151	0.523	0.523	35.76	-143	30.36	-121	-152	-182	-212
Average														31.18												
s.d.														0.63												

¹Sample name includes the grass species (Hyp for Hyparrhenia involucrata and Andro for Andropogon gayanus) and the sampling date (with DD.MM.YY)

²Rainwater average amount-weighted for the growth season preceding the sampling (1.5 and 5 months preceding September 2018 and May 2019, respectively)

³According to Dodd and Sharp (2010)

⁴According to Sharp et al. (2016)



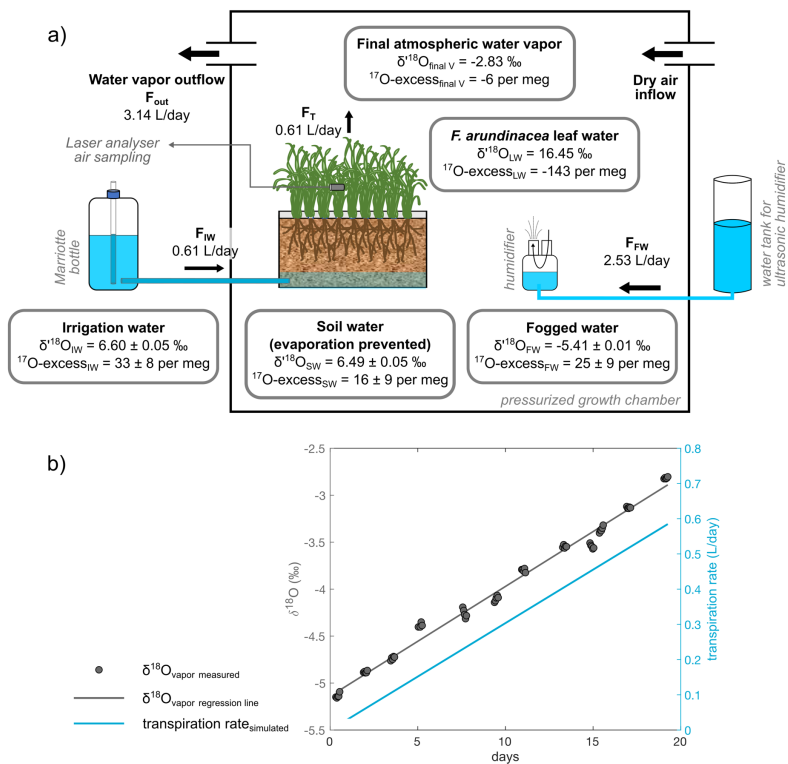
Figure captions

715 **Figure 1:** (a) Scheme of the growth chamber setup for the isotope monitoring of the water compartments in the soil-plant-atmosphere continuum. Isotope data are given for the final state of the P2-40-120717 regrowth as an example (data from Sup. mat. 1.1). The vapor outflux in humid air (F_{out}) is equal to the sum of the fogged water influx ($F_{fog\ w}$) and the irrigation water influx (F_{iw}) equivalent to the transpired water flux (T). $F_{fog\ w}$ is adjusted to keep a constant the relative humidity (RH). (b) Linear correlation with the number of growing days of the atmospheric vapor $\delta^{18}O$ ($\delta^{18}O_v$) in the growth chamber. $\delta^{18}O$ values of the initial and final water vapor ($\delta^{18}O_{initial\ v}$ and $\delta^{18}O_{final\ v}$ in Sup.mat. 1.1) were extrapolated from this correlation. The
720 transpiration rate can be calculated on a daily basis using $\delta^{18}O_v$ and the isotope mass balance equation detailed in Sup. mat. 1.1.

Figure 2: Impact of VPD changes associated with relative humidity (RH), air temperature (T_{air}) and CO_2 concentration (CO_2) changes on $\delta^{18}O$ and ^{17}O -excess values of leaf water and phytoliths. Error bars on the measurement replicates are smaller than the symbols.

725 **Figure 3:** Observed vs predicted $\delta^{18}O$ and ^{17}O -excess of leaf water for the relative humidity (RH), air temperature (T_{air}) and CO_2 concentration (CO_2) treatments of the current experiment and the RH treatment of the 2018 growth chamber experiment (recalculated from Alexandre et al., 2018). Predicted $\delta^{18}O$ and ^{17}O -excess values are reported in Sup. mat. 1.2.

Figure 4: ^{17}O -excess vs $\delta^{18}O$ of irrigation water (IW), final water vapor (V), bulk leaf water (LW), phytolith (phyto) and phytolith-forming water (FW) observed and predicted for the current and 2018 relative humidity (RH) treatment where RH varies from 40 to 60 and 80%. Phytolith-forming water values are predicted using equilibrium $^{18}O_{Silica-water}$ estimated from
730 Dodd and Sharp (2010) and $\lambda_{Silica-water}$ values of 0.524 (Sharp et al., 2016) and 0.522 (Sup. mat. 1.3). For comparison, values from the 2018 natural transect dataset (Alexandre et al., 2018) and from the AMMA-CATCH grass stem phytoliths and rainwater (RW) data (Table 3) are plotted.



735

Figure 1

740

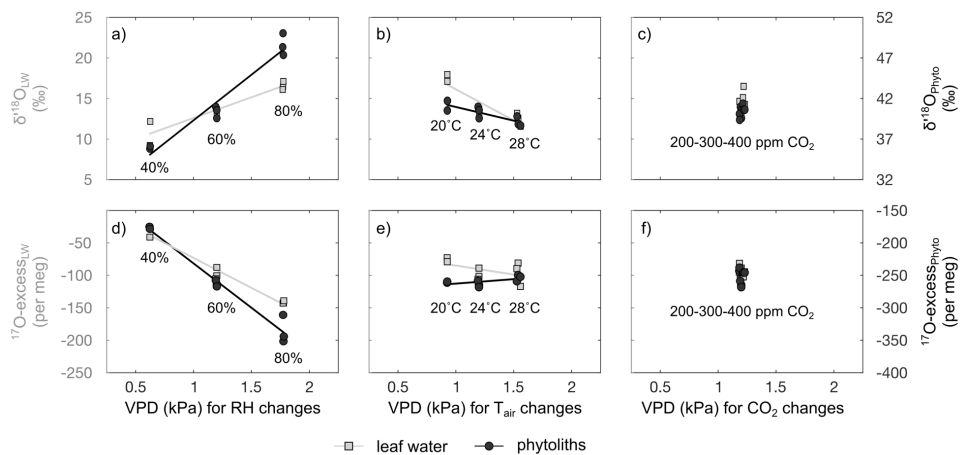


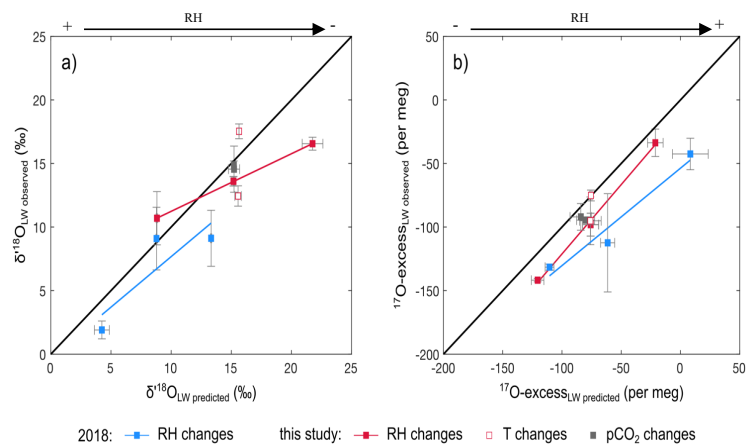
Figure 2



745

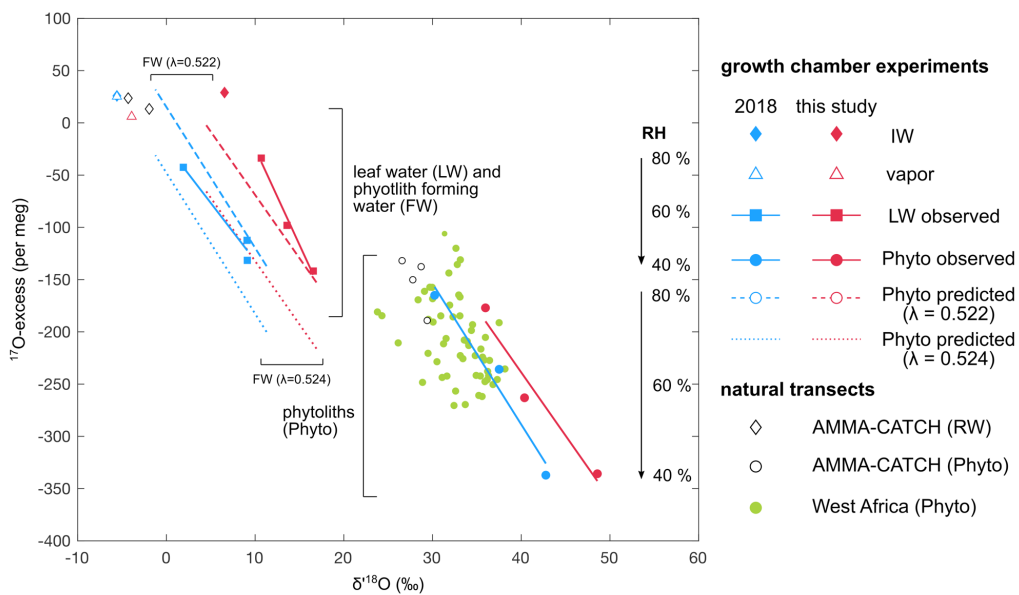
750

755



760

Figure 3



765

Figure 4